(1986). Self-inactivating retroviral vectors designed for transfer of whole genes into mammalian cells. Proc. Natl. Acad. Sci. U.S.A. 83, 3194–3198.

Yu, S.S., Han, E., Hong, Y., Lee, J.T., Kim, S., and Kim, S. (2003). Construction of a retroviral vector production system with the minimum possibility of a homologous recombination. Gene Ther. 10, 706–711.

Zhang, Y., Zhang, J., Hoeflich, K.P., Ikura, M., Qing, G., and Inouye, M. (2003). MazF cleaves cellular mRNAs specifically at ACA to block protein synthesis in *Escherichia coli*. Mol. Cell 12, 913–923.

Zhu, L., Zhang, Y., The, J.S., Zhang, J., Connell, N., Rubin, H., and Inouye, M. (2006). Characterization of mRNA interferases from Mycobacterium tuberculosis. J. Biol. Chem. 281, 18638–18643.

Zhu, L., Inoue, K., Yoshizumi, S., Kobayashi, H., Zhang, Y., Ouyang, M., Kato, F., Sugai, M., and Inouye, M. (2009). *Staphylococcus aureus* MazF specifically cleaves a pentad sequence, UACAU, which is unusually abundant in the mRNA for pathogenic adhesive factor SraP. J. Bacteriol. 191, 3248–3255.

Address correspondence to:
Dr. Ikunoshin Kato
Center for Cell and Gene Therapy
Takara Bio Inc.
Seta 3-4-1
Otsu, Shiga
520-2193, Japan

E-mail: ikukatiku@zeus.eonet.ne.jp

Dr. Masayori Inouye
Department of Biochemistry
Robert Wood Johnson Medical School
675 Hoes Lane
Piscataway, NJ 08854, USA

E-mail: inouye@umdnj.edu

Received for publication January 5, 2010;
accepted after revision July 22, 2010.

Published online: July 22, 2010.

J. Comp. Path. 2011, Vol. 144, 204–211

Available online at www.sciencedirect.com

ScienceDirect

ELSEVIER
www.elsevier.com/locate/jcpa

SHORT PAPER

Periventricular Leucomalacia (PVL)-like Lesions in Two Neonatal Cynomolgus Monkeys (*Macaca fascicularis*)

S. Okabayashi*,†, K. Uchida‡, H. Nakayama‡, C. Ohno*, K. Hanari*, I. Goto* and Y. Yasutomi†

** Corporation for Production and Research of Laboratory Primates, Hachimandai 1-1, Tsukuba-shi, Ibaraki 305-0843, † Tsukuba Primate Research Center, National Institute of Biomedical Innovation, Hachimandai 1-1, Tsukuba-shi, Ibaraki 305-0843 and ‡ Laboratory of Veterinary Pathology, Graduate School of Agricultural and Life Sciences, The University of Tokyo, Yayoi 1-1-1, Bunkyo-ku, Tokyo 113-8657, Japan*

Summary

Periventricular leucomalacia (PVL) is a lesion of immature cerebral white matter that occurs in the perinatal period. In man, PVL is the predominant form of brain injury and a cause of cerebral palsy and cognitive deficits in premature infants. PVL affects fetuses and newborns, particularly those who have undergone oxygen deprivation as may occur in premature birth. Many clinical and pathological studies of PVL have been performed in man, but there is no clear definition of PVL in animals. A few spontaneous PVL-like cases in puppies or experimental cases in other animal species have been reported. The present study reports the histopathological and immunohistochemical features of PVL-like lesions in two neonatal cynomolgus monkeys. In both cases, there was cerebral white matter necrosis with marked infiltration of lipid-laden phagocytes and a reduction of neurons in the cerebral cortex. In case 1 there was extensive cavitation of the cerebral white matter. In case 2 there was reactive astrocytosis associated with a decrease in oligodendroglial cells and a decrease in cerebral white matter myelin. To our knowledge, this is the first report of PVL-like leucoencephalomalacia in non-human primates.

Keywords: cynomolgus monkey; histopathology; immunohistochemistry; periventricular leucomalacia

Cerebral white matter injury in premature human infants is a problem of major clinical importance. These injuries take the form of multiple different lesions including intraventricular haemorrhage, post-haemorrhagic hydrocephalus and periventricular leucomalacia (PVL). PVL is the major form of cerebral white matter injury that affects premature infants and is associated with the subsequent development of cerebral palsy. The characteristic lesion of PVL consists of focal periventricular necrosis, with subsequent cyst formation and more diffuse cerebral white matter injury (Khwaja and Volpe, 2008). Although the pathogenesis of PVL remains to be completely elucidated, it is likely that the necrosis of white matter relates to impaired perfusion resulting from hypoxia–ischaemia (Khwaja and Volpe, 2008). An alternative hypothesis proposes that the lesions result from intrauterine infection with direct toxic effects on fetal oligodendrocytes and astrocytes by cytokines (Damman and Levinton, 1997). Risk factors for PVL include prematurity, asphyxia, respiratory distress, septicaemia, chorioamnionitis, arterial hypotension and hypocarbia (Resch *et al.*, 2004).

There is no clear definition of PVL in animals; however, animal models are necessary for understanding the mechanism of PVL in man. Although a few spontaneous PVL-like cases have been described in puppies (Rentmeister *et al.*, 2004) and several experimental cases (Young *et al.*, 1982; Levison *et al.*, 2001; Brazel *et al.*, 2004) have been reported, no model

Correspondence to: S. Okabayashi (e-mail: okarin@primate.or.jp).

0021-9975/$ - see front matter
doi:10.1016/j.jcpa.2010.06.006

reliably replicates all aspects of human PVL. Non-human primates have motor functions and cognitive abilities similar to man and have therefore become increasingly important as experimental models for the study of human central nervous system (CNS) disease. However, PVL-like disease has yet to be described in non-human primates. Here, we report two spontaneously arising cases of PVL-like lesions in neonatal cynomolgus monkeys (*Macaca fascicularis*).

Case 1 was a neonatal female cynomolgus monkey from the Tsukuba Primate Research Center (TPRC) that was delivered by caesarean section at 163 days of gestation as the mother had difficulties in parturition associated with profuse vaginal haemorrhage. The neonate did not breathe for several minutes, but was successfully resuscitated. The body weight of the monkey was 290 g and the animal was artificially nursed. Three days later, paralysis of the limbs was observed and the monkey became progressively debilitated due to insufficient sucking of milk. Despite treatment with subcutaneous infusion of 5% glucose solution and emergency medical care, the monkey died naturally 21 days after birth.

Case 2 was a neonatal male cynomolgus monkey born in the TPRC 16 days prior to the expected date of confinement. The mother rejected the neonate and artificial nursing was conducted. Despite the preterm birth, the body weight of this monkey was 290 g (the average weight of neonatal cynomolgus monkeys in the TPRC is approximately 300–350 g). The next day, paralysis of the limbs was observed and the monkey could not suck sufficient milk. Because this monkey had abnormal breath sounds 3 days after birth, the veterinarian continued treatment with subcutaneous infusion of 5% glucose solution and antibiotics. However, the monkey died naturally 7 days after birth.

Necropsy examination was performed in each case. Tissues were fixed in 10% neutral buffered formalin, processed routinely and embedded in paraffin wax. Sections (3 μm) were stained with haematoxylin and eosin (HE). For immunohistochemistry (IHC), dewaxed sections were pretreated with H_2O_2 0.5% in methanol and then subjected to antigen retrieval by immersion in citric acid buffer (pH 6.0) and heating in an autoclave for 10 min at 121°C. Sections were then incubated free floating in primary antibody solution overnight at 4°C. Primary antibodies were mouse monoclonal antibodies specific for glial fibrillary acidic protein (GFAP, clone LF2, Dako, Glostrup, Denmark; 1 in 200 dilution), CD68 (clone KP1, Dako; 1 in 100 dilution), vimentin (clone 3B4, Dako; 1 in 200 dilution), neurofilament (NF, clone 2F11, Dako; 1 in 100 dilution) and active-caspase-3 (Cas3; Chemicon, Temecula, California; 1 in 100 dilution). Following brief washes with buffer, the sections were incubated sequentially with polymer immunocomplex (Dako) for 30 min. Immunoreactive elements were 'visualized' by treating the sections with 3, 3′-diaminobenzidine tetroxide (Dojin Kagaku, Kunamoto, Japan) followed by counterstaining with haematoxylin.

For double immunolabelling, sections were dewaxed and then stained with 1% Sudan black B to reduce autofluorescence. Following brief washes, sections were incubated free floating overnight at 4°C in solutions containing mouse monoclonal antibody for myelin basic protein (MBP; Chemicon; 1 in 500 dilution) and rabbit polyclonal antibody specific for oligodendrocytes (olig2; IBL, Takasaki, Gunma, Japan; 1 in 500 dilution). Sections were then incubated with AlexaFluor 488-conjugated goat anti-mouse IgG (Invitrogen, Carlsbad, California; 1 in 1,000 dilution) and AlexaFluor 555-conjugated goat anti-rabbit IgG (Invitrogen; 1 in 1,000 dilution) for 1 h at room temperature. The sections were examined with a Digital Eclipse C1 confocal microscope (Nikon, Kanagawa, Japan). Neonatal monkey brain sections (0-day-old animals) were used as normal controls.

Grossly, the neonatal monkeys were emaciated, dehydrated and had pale mucous membranes. Both limbs and the tail had a decreased range of motion and atrophy of limb muscles was observed in each case. Both tracheas were filled with mucus mixed with milk. The lungs were oedematous and hyperaemic and there were several small white nodules (2–3 mm diameter) in all pulmonary lobes in case 2. In case 1, an excessive quantity of cerebrospinal fluid (CSF) had accumulated in the cranial cavity and the volume of the cerebrum appeared reduced. After formalin fixation, cross sections of the cerebrum in case 1 revealed the presence of marked cavitation of the white matter and atrophy of the cortical region (Fig. 1A), whereas multiple foci of softening of the white matter were found in cross sections of the cerebrum in case 2 (Fig. 1B).

Microscopically, in case 1 areas of cavitation or foci of liquefactive necrosis were widespread with loss of all cellular elements from white matter to deep gray matter, with many lipid-filled phagocytes aggregated within the necrotic foci (Fig. 2A). Residual cerebral cortex showed marked reduction in the number of neural cells. The lateral ventricle was enlarged, with hyperaemia of the choroid plexus, and the ependymal layers showed glial cell infiltration and partial exfoliation. Glial cell infiltration, glial nodules and aggregation of lipid-filled phagocytes with formation of cholesterol clefts were found in the periventricular regions of the lateral ventricle. However, the

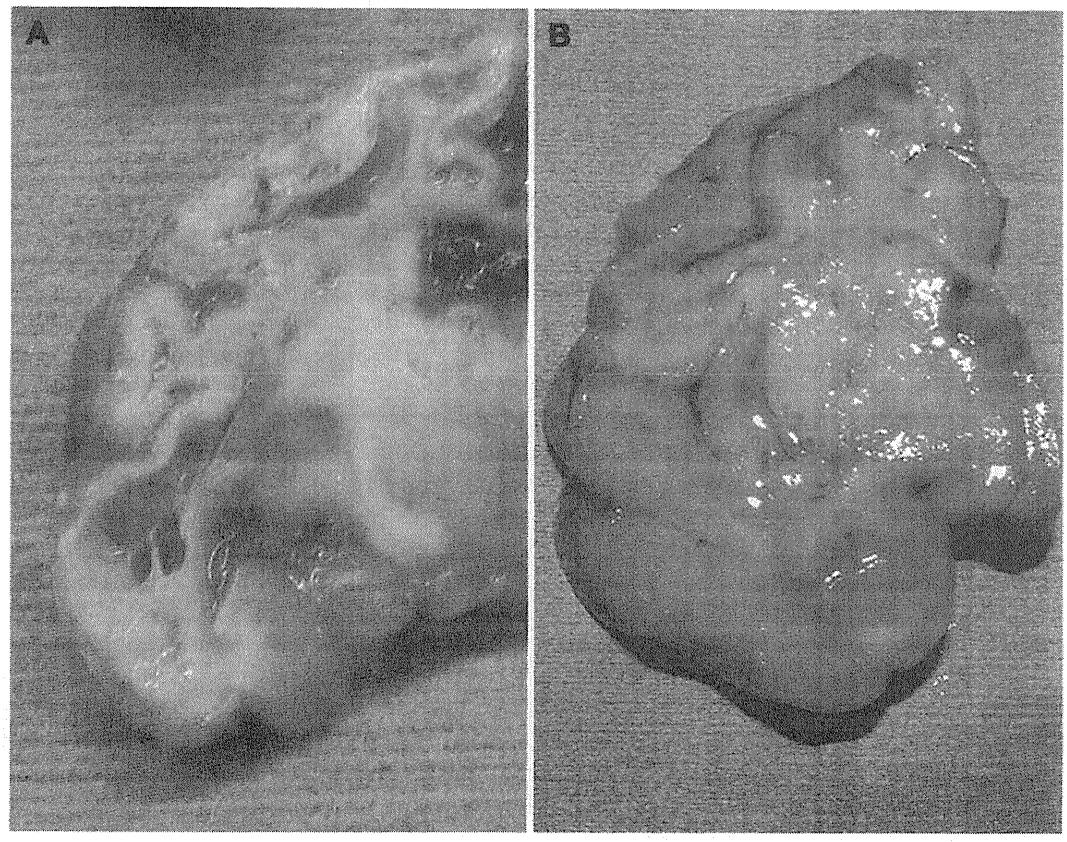

Fig. 1. (A) Cerebrum of a 21-day-old cynomolgus monkey (case 1). Marked cavitation of the white matter and atrophy of the cortical region are present in the temporal lobe. (B) Cerebrum in a 7-day-old cynomolgus monkey (case 2). Multiple foci of white matter softening are present in the temporal lobe.

periventricular regions and ependymal layers of the third ventricle appeared to be largely normal, except for a slight infiltration of glial cells. In case 2, the cerebrum showed massive liquefactive necrosis, with infiltration of lipid-filled phagocytes bilaterally in the temporal white matter and particularly in the periventricular areas of the lateral ventricle. Furthermore, there was diffuse reactive astrocytosis with gemistocytes (Fig. 3A) in various white matter areas and focally in the temporal deep gray matter. The density of neuronal cells was significantly reduced in the lesional sites. Periventricular areas of the third ventricle and thalamus also showed a decrease in neurons infiltration of lipid-filled phagocytes and astrocytosis. Examination of the brainstem, cerebellum, spinal cord and optic nerves did not reveal any abnormalities in either case.

In case 1, immunohistochemical labelling for expression of GFAP revealed apparent proliferation of glial fibrils in the cerebral cortex around cavitations or foci of liquefactive necrosis consistent with glial scar formation (Fig. 2B). In case 2, gemistocytes in the cerebral white matter displayed strong cytoplasmic immunoreactivity for GFAP (Fig. 3A). Immature astrocytes with narrow cytoplasm and long processes were immunolabelled for GFAP and vimentin (Fig. 3B) in the cerebral cortex and the cerebral white matter. Lipid-filled phagocytes in necrotic foci displayed granular cytoplasmic immunoreactivity for CD68 in both cases (Fig. 2A). Neurons displaying immunoreactivity for NF were significantly reduced in number in each case. Both cases were negative for Cas3 expression, suggesting that the lesions were a result of necrosis rather than apoptosis. Double immunohistochemical labelling with anti-MBP and anti-olig2 was also performed. In normal neonatal monkey brains, some oligodendroglial cells and many myelin sheaths were observed in the white matter (Fig. 4). In contrast, the white matter in case 2 showed a marked decrease in oligodendroglial cells and myelin sheaths (Fig. 4). The white matter in case 1 was unlabelled due to loss of all cellular elements within the areas of cavitation.

In case 1, the lung showed alveolar collapse with proliferation of type II alveolar epithelial cells (AEC II) and infiltration of macrophages into the alveolar space. In case 2, the lung showed severe diffuse pneumonia with infiltration of neutrophils and macrophages into the alveolar space and exfoliation of the alveolar epithelium.

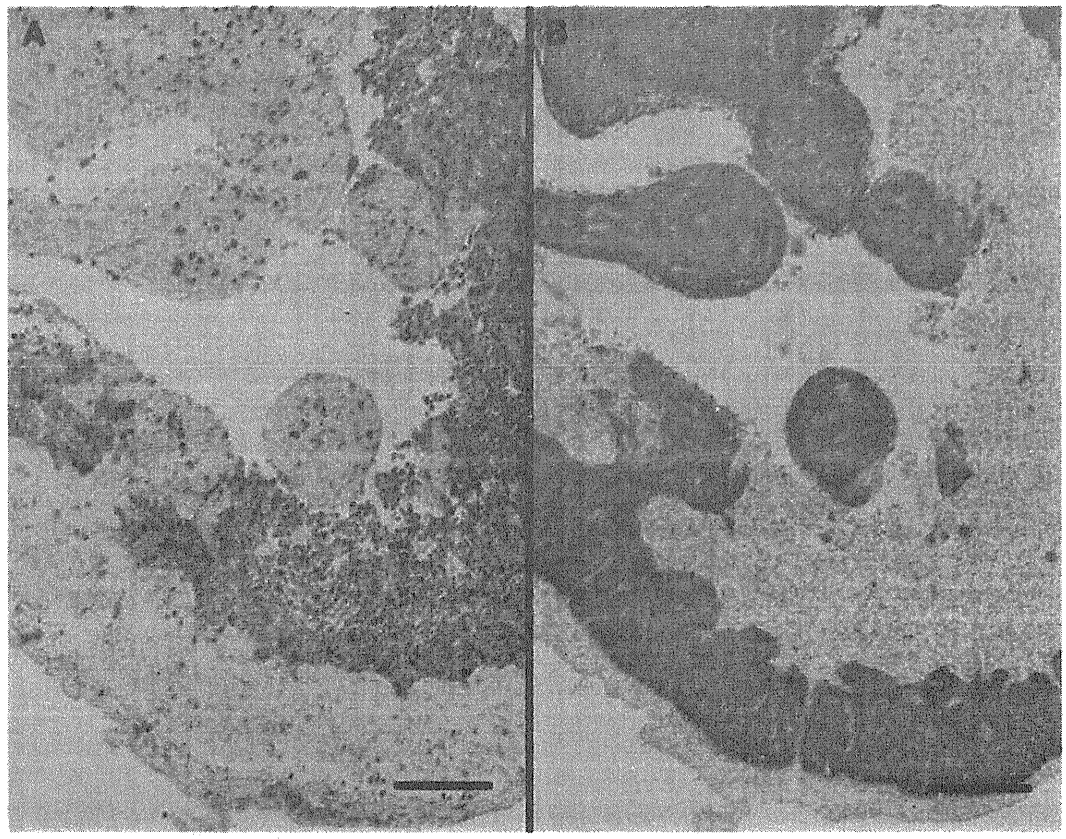

Fig. 2. Cerebrum of a 21-day-old cynomolgus monkey (case 1). (A) There is cavitation or foci of liquefactive necrosis with loss of all cellular elements from white matter to deep gray matter, with aggregation of many lipid-filled phagocytes expressing CD68 in the necrotic foci. IHC. Bar, 200 μm. (B) There is apparent proliferation of glial fibrils around these areas of cavitation or liquefactive necrosis. IHC. Bar, 200 μm.

Some colonies of gram-positive bacteria with morphology consistent with *Staphylococcus* were also observed within the white nodules in the lungs. Additionally, gastric contents, including milk, were found in the trachea of both cases. Atrophy of femoral muscles was observed with proliferation of stromal connective tissue in each case, and this change was particularly severe in case 1. The sciatic nerves of both monkeys appeared almost normal, but there was proliferation of surrounding perineural connective tissue.

Brain injury in the premature human infant consists of multiple lesions, principally germinal intraventricular haemorrhage, post-haemorrhagic hydrocephalus and PVL (Volpe, 2003). PVL refers to injury of the cerebral white matter that occurs with characteristic distribution and consists of focal periventricular necrosis with subsequent cyst formation (cystic PVL) and more diffuse cerebral white matter necrosis with subsequent glial scaring (non-cystic PVL). A third form of cerebral white matter abnormality (the third form of PVL) consists of diffuse astrogliosis without necrosis (Khwaja and Volpe, 2008). PVL is the major form of brain white matter injury that affects premature human infants and is associated with subsequent development of cerebral palsy, intellectual impairment and visual disturbances. There is currently no specific therapy for PVL (Pierson *et al.*, 2007). The diagnostic hallmarks of PVL are periventricular echodensities or cysts detected by cranial ultrasonography (Deng *et al.*, 2008). Two major factors appear to be involved in the development of PVL. The first involves fetal or neonatal hypoxia–ischaemia that can be a consequence of reduced blood flow to the umbilicus, uterus or placenta in the prenatal or perinatal period. Recent studies suggest that a disturbance of circulation, such as severe hypotension, or cardiogenic shock in preterm infants, such as caused by severe perinatal asphyxia, plays a decisive role in the formation of PVL-lesions (Shankaran *et al.*, 2006; Khwaja and Volpe, 2008). Moreover, experimental studies in which hypoxia is induced artificially have been also conducted in animals for exploration of the pathophysiology of PVL (Painter, 1995; Kohlhauser *et al.*, 2000). Anatomically, early in development, the deep penetrating arteries of the middle cerebral artery that supply the periventricular white matter lack the

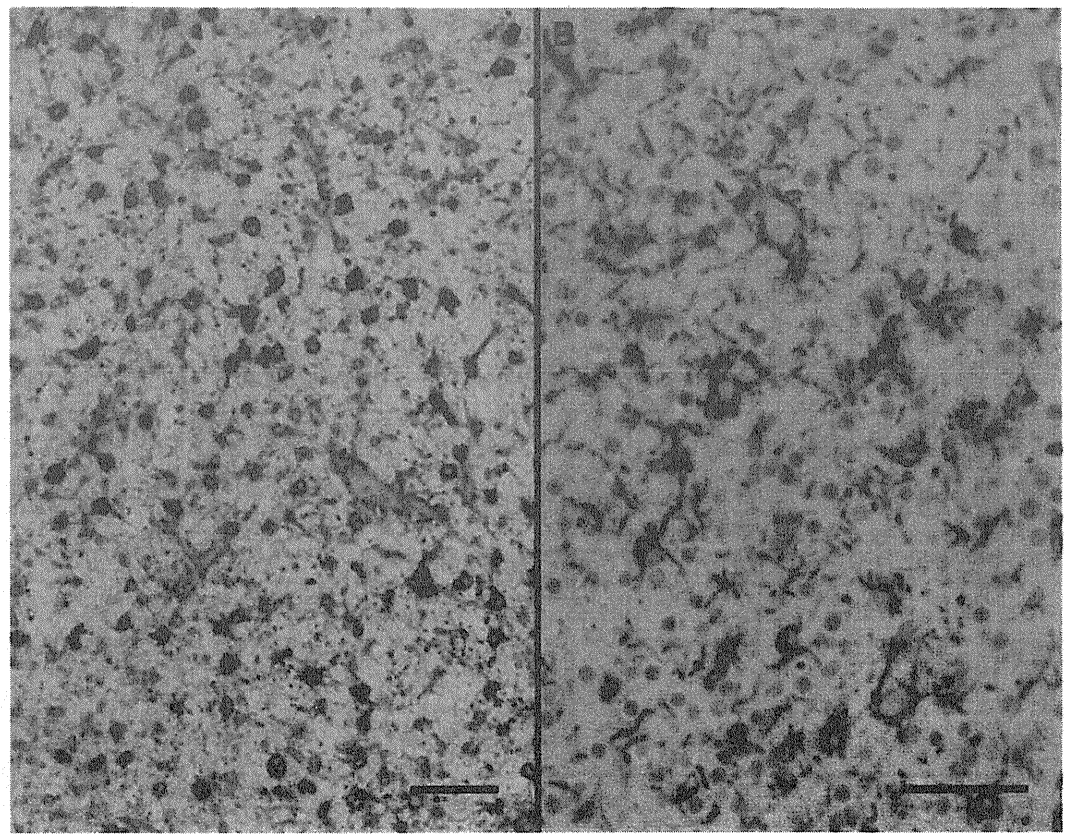

Fig. 3. Cerebrum of a 7-day-old cynomolgus monkey (case 2). (A) Large numbers of reactive astrocytes are present in the cerebral white matter. The cytoplasm of these cells labels for expression of GFAP, an astrocyte-specific marker. IHC. Bar, 50 μm. (B) Premature astrocytes are also present in the cerebral cortex. The narrow cytoplasm and long processes of these cells were immunolabelled for expression of vimentin. IHC. Bar, 50 μm.

vascular anastomoses that help maintain perfusion during periods of hypotension (Takashima *et al.*, 1978; Rorke, 1992; Inage *et al.*, 2000). Therefore, as cerebral autoregulation begins to fail following severe hypotension in neonatal infants, particularly in preterm infants, blood flow is selectively impaired and initially in the white matter of the periventricular region. Furthermore, there is recent evidence that the brain of sick preterm infants often shows impaired cerebrovascular autoregulation in response to change in blood pressure (Soul *et al.*, 2007). This selective hypoperfusion of cerebral white matter during severe hypotension provides a mechanistic explanation for the pathogenesis of PVL. Meanwhile, microglia are activated by the release of reactive oxygen species (ROS) and reactive nitrogen species (RNS), which may mediate cell death. The reactive astrocytes in diffuse lesions could also contribute to the formation of RNS. The release of ROS and RNS by microglia seems likely to result in death of premyelinating oligodendrocytes (pre-OLs) or prevent pre-OLs from differentiating to mature myelin-producing cells in the injured cerebral white matter (Volpe, 2003; Khwaja and Volpe, 2008).

The second major factor contributing to the development of PVL is thought to be maternal intrauterine (or neonatal) infection and fetal (or neonatal) systemic inflammation. Increasing numbers of studies have implicated intrauterine infection in the genesis of PVL. Recent investigations have shown that intravenous injection of the bacterial endotoxin lipopolysaccharide (LPS) can produce selective white matter injury in the neonatal CNS (Paintlia *et al.*, 2008), whereas induction of intrauterine infection can produce diffuse glial cell death and cavitation in fetal white matter (Sherwin and Fern, 2005). The secretion of proinflammatory cytokines such as interleukin (IL)-1, IL-6, and tumor necrosis factor (TNF)-α is known to be toxic to the developing fetal brain (Damman and Levinton, 1997) and may lead to astrogliosis affecting the maturation of myelin-forming oligodendrocytes (Leviton and Gilles, 1996).

The gestation period of the cynomolgus monkey averages 165 days in the TPRC. Case 1 was born on day 163 of gestation and was thus of normal gestational age; however, this animal suffered from a period of asphyxia due to perinatal dystocia. Perinatal asphyxia results from oxygen deprivation that may

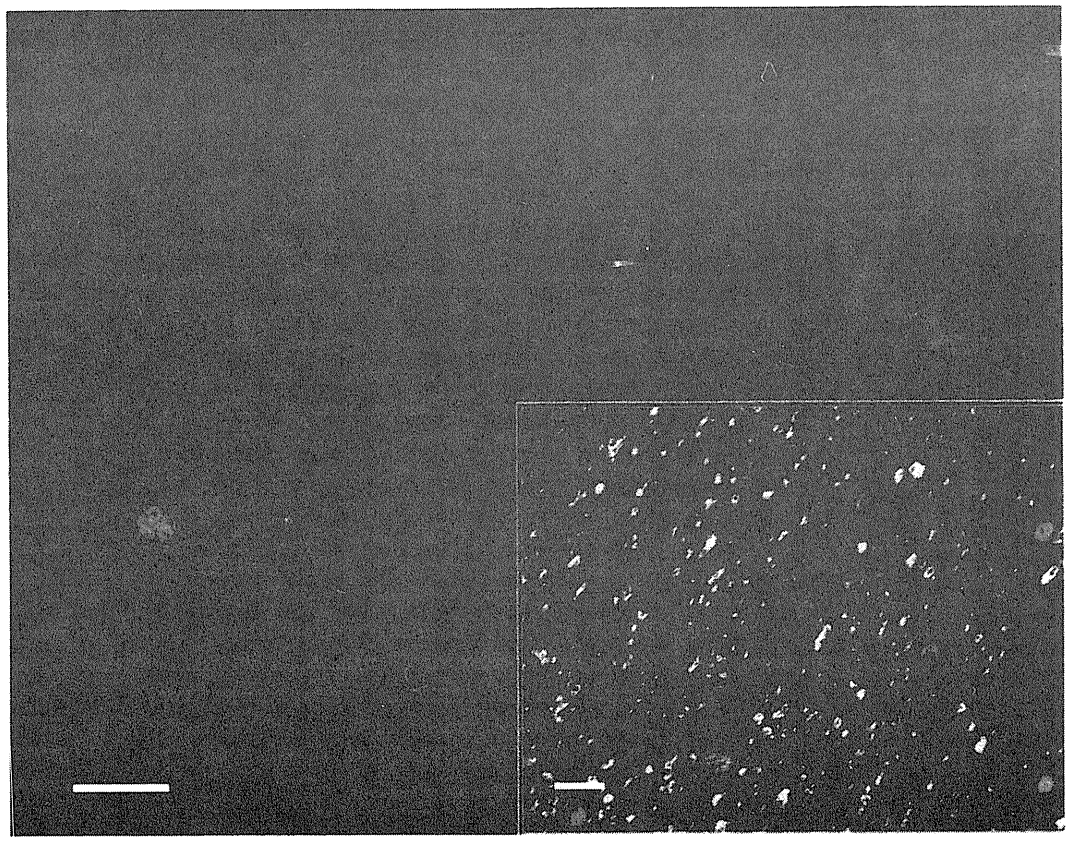

Fig. 4. Cerebrum of a 7-day-old cynomolgus monkey (case 2). Sections were double labelled with antibodies specific for MBP (green) and olig2 (red). There is reduction in cells expressing olig2 and almost no expression of MBP in the cerebral white matter. IHC. Bar, 10 μm. Inset: cerebrum of a normal 0-day-old cynomolgus monkey double labelled as above (control). Within the white matter, oligodendroglial cells express olig2 and many myelin sheaths express MBP. IHC. Bar, 10 μm.

cause harm to the neonatal infant. The condition occurs most commonly due to a drop in maternal blood pressure or interference with blood flow to the brain of the infant during delivery. This was likely to have been the aetiology of the lesions observed in the brain of case 1.

Case 2 was born 16 days before the expected date of confinement. Although PVL may occur in term infants, the injury is more common in premature infants, especially those born between 26 and 34 weeks of gestation (Locatelli *et al.*, 2005). The brain injury in preterm infants is mainly due to the oxidative stress placed on the neonate during delivery (Robles *et al.*, 2001; Haynes *et al.*, 2005), the immaturity of the developing nervous system, and the immaturity of the cerebrovascular supply (Khwaja and Volpe, 2008). Robles *et al.* (2001) investigated the concentration of hydroperoxides, which are measures of oxidative stress. These authors demonstrated that full-term neonates had levels of hydroperoxides that dropped sharply in the first few hours following birth. However, in premature infants the concentration of hydroperoxides remained at near birth levels for as long as a week and at dangerously high levels for even longer. Therefore, preterm neonates are at risk of free-radical injury during this period. In addition to these underlying factors, hypoxia–ischaemia can lead to more free-radical production, which can then damage the pre-OLs (Yoshida-Shuto *et al.*, 1992; Robles *et al.*, 2001). Thus, case 2 was at risk of a nervous system disorder and was of especially high risk for developing PVL. A genetic susceptibility to PVL has been proposed with cytokine genes acting as risk modifiers (Baier, 2006), but there was no familial association between the two animals of the present report.

Case 1 had marked cavitation with loss of cellular elements in the cerebral white matter. These changes are similar to cystic PVL and the cavitations may be formed by fusion of multiple cystic foci. Case 2 did not show cavitation, despite the presence of diffuse necrosis of the cerebral white matter, astrogliosis, decreased oligodendroglial cells and marked dysmyelination. These changes are similar to non-cystic PVL or the third form of PVL, and dysmyelination must have been caused by a decrease of myelin-producing oligodendrocytes and disturbance of pre-OL maturation.

The pathological differences between the two monkeys may also have been influenced by the duration of ischaemia or other factors such as fetal age or the length of survival. In general, it is said that microglial reactivity is apparent within 24 h, peaks at 7 days and remains present for weeks following the ischaemia. Phenotypic changes in resident astrocytes occur at 24 h, and these cells proliferate between 48 h and 7 days after ischaemia. Over the ensuing weeks and months, astrocytes increase in number and in fibrillary appearance, eventually resulting in a glial scar or cavitation (Cervós-Navarro and Lafuente, 1991; Williams *et al.*, 2007). Case 1 had widespread cavitation and severe glial scarring, while case 2 showed neuronal decrease, infiltration of lipid-filled phagocytes and astrocytosis in the cerebral white matter and the thalamus. The thalamus is commonly affected in premature infants with PVL (Volpe, 2009), therefore the thalamic lesion in case 2 may have been linked to preterm birth. Furthermore, in each case the femoral muscles showed apparent neurogenic atrophy, likely secondary to dysfunction of the cerebral white matter.

Both monkeys had diffuse pulmonary lesions. In case 1, alveolar collapse was observed with proliferation of AEC II. This may have been caused by artificial ventilation and inhalation of highly concentrated oxygen administered as part of the medical care of the animal. Hyperoxia or hypocarbia results in the death of AEC I and subsequent proliferation of AEC II that differentiate to AEC I to replace the injured or dead AECs during the recovery stages (Takemura and Akamatsu, 1987). Case 2 showed severe purulent alveolar pneumonia with bacterial infection. This bacterial pneumonia may have been due to compromise of the immune system or decreased strength in this premature infant. Both tracheas were filled with a mixture of milk and mucus, suggesting that the animals may have terminally aspirated gastric contents.

Criteria for PVL in animals have not been defined, but the clinical and pathological features of our cases were very similar to those of PVL in man. TPRC has a large-scale breeding colony of experimental cynomolgus monkeys, with about 200 births each year. However, these are the first cases experienced in the TPRC and the first from any primate centre. Future cases should also be subject to ultrasonographic or magnetic resonance imaging investigation. Brain injury in premature infants has an enormous importance to public health because of the large number of such infants who survive with serious neurodevelopmental disability, including major cognitive deficits and motor disability. Because man and monkeys are very similar in anatomy, motor function and cognitive ability, monkeys are favoured as non-human primate models for the study of post-injury changes in the CNS. These spontaneously arising cases in non-human primates will contribute greatly to understanding the pathophysiology of PVL and to the development of an effective therapy for PVL or cerebral palsy.

Acknowledgments

This study was supported by the Tsukuba Primate Research Center, National Institute of Biomedical Innovation, Japan.

References

Baier RJ (2006) Genetics of perinatal brain injury in the preterm infant. *Frontiers in Biosciences*, **11**, 1371–1387.

Brazel CY, Rosti RT, Boyce S, Rothstein RP, Levison SW (2004) Perinatal hypoxia/ischemia damages and depletes progenitors from the mouse subventricular zone. *Developmental Neuroscience*, **26**, 266–274.

Cervós-Navarro J, Lafuente JV (1991) Traumatic brain injuries: structural changes. *Journal of Neurological Science*, **103**, S3–S14.

Damman O, Levinton A (1997) Maternal intrauterine infection, cytokines, and brain damage in the preterm newborn. *Pediatric Research*, **42**, 1–8.

Deng W, Pleasure J, Pleasure D (2008) Progress in periventricular leukomalacia. *Archives of Neurology*, **65**, 1291–1295.

Haynes RL, Baud O, Li J, Kinney HC, Volpe JJ *et al.* (2005) Oxidative and nitrative injury in periventricular leukomalacia: a review. *Brain Pathology*, **15**, 225–233.

Inage YW, Itoh M, Takashima S (2000) Correlation between cerebrovascular maturity and periventricular leukomalacia. *Pediatric Neurology*, **22**, 204–208.

Khwaja O, Volpe JJ (2008) Pathogenesis of cerebral white matter injury of prematurity. *Archives of Disease in Childhood. Fetal and Neonatal Edition*, **93**, 153–161.

Kohlhauser C, Mosgöller W, Höger H, Lubec B (2000) Myelination deficits in brain of rats following perinatal asphyxia. *Life Sciences*, **67**, 2355–2368.

Levison SW, Rothstein RP, Romanko MJ, Snyder MJ, Meyers RL *et al.* (2001) Hypoxia/ischemia depletes the rat perinatal subventricular zone of oligodendrocyte progenitors and neural stem cells. *Developmental Neuroscience*, **23**, 234–247.

Leviton A, Gilles F (1996) Ventriculomegaly, delayed myelination, white matter hypoplasia, and 'periventricular' leukomalacia: how are they related? *Pediatric Neurology*, **15**, 127–136.

Locatelli A, Ghidini A, Paterlini G, Patanè L, Doria V *et al.* (2005) Gestational age at preterm premature rupture of membranes: a risk factor for neonatal white matter damage. *American Journal of Obstetrics and Gynecology*, **193**, 947–951.

Painter MJ (1995) Animal models of perinatal asphyxia: contributions, contradictions, clinical relevance. *Seminars in Pediatric Neurology*, **2**, 37–56.

Paintlia MK, Paintlia AS, Contreras MA, Singh I, Singh AK (2008) Lipopolysaccharide-induced

peroxisomal dysfunction exacerbates cerebral white matter injury: attenuation by N-acetyl cysteine. *Experimental Neurology*, **210**, 560–576.

Pierson CR, Folkerth RD, Billiards SS, Trachtenberg FL, Drinkwater ME *et al.* (2007) Gray matter injury associated with periventricular leukomalacia in the premature infant. *Acta Neuropathology*, **114**, 619–631.

Rentmeister K, Schmidbauer S, Hewicker-Trautwein M, Tipold A (2004) Periventricular and subcortical leukoencephalopathy in two dachshund puppies. *Journal of Veterinary Medicine Series A: Physiology, Pathology and Clinical Medicine*, **51**, 327–331.

Resch B, Jammernegg A, Vollaard E, Maurer U, Mueller WD *et al.* (2004) Preterm twin gestation and cystic periventricular leucomalacia. *Archives of Disease in Childhood. Fetal and Neonatal Edition*, **89**, F315–320.

Robles R, Palomino N, Robles A (2001) Oxidative stress in the neonate. *Early Human Development*, **65**, S75–S81.

Rorke LB (1992) Anatomical features of the developing brain implicated in pathogenesis of hypoxic-ischemic injury. *Brain Pathology*, **2**, 211–221.

Shankaran S, Langer JC, Kazzi SN, Laptook AR, Walsh M (2006) Cumulative index of exposure to hypocarbia and hyperoxia as risk factors for periventricular leukomalacia in low birth weight infants. *Pediatrics*, **118**, 1654–1659.

Sherwin C, Fern R (2005) Acute lipopolysaccharide-mediated injury in neonatal white matter glia: role of TNF-alpha, IL-1beta, and calcium. *Journal of Immunology*, **175**, 155–161.

Soul JS, Hammer PE, Tsuji M, Saul JP, Bassan H *et al.* (2007) Fluctuating pressure-passivity is common in the cerebral circulation of sick premature infants. *Pediatric Research*, **61**, 467–473.

Takashima S, Armstrong DL, Becker LE (1978) Subcortical leukomalacia. Relationship to development of the cerebral sulcus and its vascular supply. *Archives of Neurology*, **35**, 470–472.

Takemura T, Akamatsu H (1987) Ultrastructural study on the pulmonary parenchyma of the neonates following prolonged mechanical ventilation. *Acta Pathologica Japonica*, **37**, 1115–1126.

Volpe JJ (2003) Cerebral white matter injury of the premature infant – more common than you think. *Pediatrics*, **112**, 176–180.

Volpe JJ (2009) Brain injury in premature infants: a complex amalgam of destructive and developmental disturbances. *Lancet Neurology*, **8**, 110–124.

Williams AJ, Wei HH, Dave JR, Tortella FC (2007) Acute and delayed neuroinflammatory response following experimental penetrating ballistic brain injury in the rat. *Journal of Neuroinflammation*, **2**, 4–17.

Yoshida-Shuto H, Yasuhara A, Kobayashi Y (1992) Cerebral blood flow velocity and failure of autoregulation in neonates: their relation to outcome of birth asphyxia. *Neuropediatrics*, **23**, 241–244.

Young RS, Hernandez MJ, Yagel SK (1982) Selective reduction of blood flow to white matter during hypotension in newborn dogs: a possible mechanism of periventricular leukomalacia. *Annals of Neurology*, **12**, 445–448.

[*Received, January 23rd, 2010*
Accepted, June 27th, 2010]

frontiers in
MICROBIOLOGY

ORIGINAL RESEARCH ARTICLE
published: 07 December 2011
doi: 10.3389/fmicb.2011.00240

Long-term persistent GBV-B infection and development of a chronic and progressive hepatitis C-like disease in marmosets

Yuki Iwasaki[1,2†], Ken-ichi Mori[3†], Koji Ishii[4], Noboru Maki[3], Sayuki Iijima[1], Tomoyuki Yoshida[5], Sachi Okabayashi[6], Yuko Katakai[6], Young-Jung Lee[1], Akatsuki Saito[5], Hiromi Fukai[3], Nobuyuki Kimura[1], Naohide Ageyama[1], Sayaka Yoshizaki[4], Tetsuro Suzuki[4], Yasuhiro Yasutomi[1], Tatsuo Miyamura[4], Mari Kannagi[2] and Hirofumi Akari[1,5]*

[1] *Tsukuba Primate Research Center, National Institute of Biomedical Innovation, Tsukuba, Japan*
[2] *Department of Immunotherapeutics, Graduate School of Medicine and Dentistry, Tokyo Medical and Dental University, Tokyo, Japan*
[3] *Advanced Life Science Institute, Wako, Japan*
[4] *Department of Virology II, National Institute of Infectious Diseases, Tokyo, Japan*
[5] *Primate Research Institute, Kyoto University, Inuyama, Japan*
[6] *Corporation for Production and Research of Laboratory Primates, Tsukuba, Japan*

Edited by:
Yasuko Yokota, National Institute of Infectious Diseases, Japan

Reviewed by:
Ikuo Shoji, Kobe University Graduate School of Medicine, Japan
Soon B. Hwang, Hallym University, South Korea

***Correspondence:**
Hirofumi Akari, Primate Research Institute, Kyoto University, Inuyama 484-8506, Japan.
e-mail: akari@pri.kyoto-u.ac.jp

†*Yuki Iwasaki and Ken-ichi Mori have contributed equally to this work.*

It has been shown that infection of GB virus B (GBV-B), which is closely related to hepatitis C virus, develops acute self-resolving hepatitis in tamarins. In this study we sought to examine longitudinally the dynamics of viral and immunological status following GBV-B infection of marmosets and tamarins. Surprisingly, two of four marmosets but not tamarins experimentally challenged with GBV-B developed long-term chronic infection with fluctuated viremia, recurrent increase of alanine aminotransferase and plateaued titers of the antiviral antibodies, which was comparable to chronic hepatitis C in humans. Moreover, one of the chronically infected marmosets developed an acute exacerbation of chronic hepatitis as revealed by biochemical, histological, and immunopathological analyses. Of note, periodical analyses of the viral genomes in these marmosets indicated frequent and selective non-synonymous mutations, suggesting efficient evasion of the virus from antiviral immune pressure. These results demonstrated for the first time that GBV-B could induce chronic hepatitis C-like disease in marmosets and that the outcome of the viral infection and disease progression may depend on the differences between species and individuals.

Keywords: GBV-B, HCV, marmoset, tamarin, hepatitis C

INTRODUCTION

Among the known viruses, GB virus B (GBV-B) is closely related to hepatitis C virus (HCV), with 25–30% homology at the amino acid level, and is tentatively classified in *Hepacivirus* genus of *Flavivirus* family (Muerhoff et al., 1995; Simons et al., 1995; Ohba et al., 1996). Due to limited epidemiological analyses, the natural host(s) and prevalence of GBV-B have remained to be determined.

Hepatitis C virus is a major causative agent for non-A, non-B hepatitis. HCV is globally disseminated and estimated to be carried by more than 170 million people (Chisari, 2005; Lavanchy, 2009). Most HCV-infected individuals develop chronic liver diseases such as liver cirrhosis and hepatocellular carcinoma (Hoofnagle, 1997; Seeff and Hoofnagle, 2002; Rehermann and Nascimbeni, 2005). Since standard therapy with PEGylated interferon and ribavirin is effective for only about 50% of patients, it is crucial to develop more effective therapeutics (Feld and Hoofnagle, 2005; Melnikova, 2008). The only validated animal model for HCV infection is the chimpanzees. This model has been valuable for determining important aspects of this disease, including the relationship between the virus and the antiviral immune responses of the host and the process of viral pathogenesis (Bukh, 2004; Akari et al., 2009; Boonstra et al., 2009). However, chimpanzees are endangered and present ethical complications and the availability of these experimental animals is severely restricted.

When tamarins (members of the New World monkeys) are infected with GBV-B, they generally develop acute viremia and self-resolving hepatitis as indicated by increases in the levels of serum enzymes such as alanine aminotransferase (ALT) (Bukh et al., 1999; Beames et al., 2000; Beames et al., 2001; Sbardellati et al., 2001; Lanford et al., 2003; Martin et al., 2003; Bright et al., 2004; Jacob et al., 2004; Nam et al., 2004; Kyuregyan et al., 2005; Ishii et al., 2007; Weatherford et al., 2009). Thus, the monkeys have been proposed as a surrogate model of HCV infection of chimpanzee and humans. However, a major hurdle for the development of a monkey-based surrogate model is the difficulties encountered in obtaining chronically infected monkeys that exhibit progression of chronic hepatitis C-like diseases (Martin et al., 2003; Nam et al., 2004; Takikawa et al., 2010).

Abbreviations: ALT, alanine aminotransferase; GBV-B, GB virus B; HCV, hepatitis C virus; HE, hematoxylin and eosin; p.i., post infection.

It has recently been shown that marmosets, another member of New World monkeys, are susceptible to GBV-B infection and develop relatively lower levels of acute viremia (10^5–10^8 copies/ml) as compared with that in tamarins (10^7–10^{10} copies/ml) (Lanford et al., 2003; Bright et al., 2004; Woollard et al., 2008; Weatherford et al., 2009), although it remains elusive whether the marmosets could permit persistent GBV-B infection. Considering that the viral loads in the acute phase of experimental HCV infection of chimpanzees that consequently develop persistent infection are generally 10^7 copies/ml or less (Fernandez et al., 2004; Bukh et al., 2008), it is possible that the lower viral loads in the acute phase is preferable for the establishment of viral persistency. We thus initiated studies of the dynamics of viral and immunological status following GBV-B infection of tamarins and marmosets in a longitudinal follow-up study. We show here for the first time that GBV-B infection produces a chronic and progressive hepatitis C-like disease in marmosets as demonstrated by fibrosis and a recurrent ALT increase and that one of the marmosets experienced acute exacerbation of chronic hepatitis as indicated by piecemeal necrosis and an ALT flare >4 years after infection.

MATERIALS AND METHODS

ANIMALS

Adult red-handed tamarins (*Saguinus midas*) and common marmosets (*Callithrix jacchus*) were housed in individual cages at the Tsukuba Primate Research Center. All animal studies were conducted in accordance with the protocols of experimental procedures that were approved by the Animal Welfare and Animal Care Committees of the National Institute of Biomedical Innovation and the National Institute of Infectious Diseases.

GBV-B INFECTION IN TAMARINS AND MARMOSETS

GBV-B infectious serum obtained from a tamarin (1.3×10^9 viral RNA copies per inoculum) was injected into each tamarin and marmoset intrahepatically as previously described (Ishii et al., 2007). We confirmed that the inoculum contained no mutations as compared with the original sequence. Of note, an anti-luciferase siRNA in a cationic liposome formulation was administered to one of the marmosets (Cj05-002) 2 days before the infection, which was performed as previously described (Yokota et al., 2007). Blood samples were periodically collected from the femoral vein of each animal under anesthesia and the plasma samples were evaluated for GBV-B genomic RNA, ALT, and antibodies against GBV-B core and NS3 proteins.

QUANTIFICATION OF GBV-B GENOMIC RNA

GBV-B RNA was isolated from the plasma samples by using a QIAamp MinElute Virus Spin kit (QIAGEN) and was quantified by real-time PCR using the 5′-exonuclease PCR (TaqMan) assay system (Ishii et al., 2007). The primers 558F [5′-AACGAGCAAAGCGCAAAGTC] and 626R [5′-CATCATGGATACCAGCAATTTTGT] and the probe 579P [5′-FAM-AGCGCGATGCTCGGCCTCGTA-TAMRA] (Beames et al., 2000) were obtained from Sigma-Aldrich. The cutoff value was 10^3 copies/ml. All the specimens were evaluated in duplicate and the average values were calculated.

DETECTION OF ANTIBODIES AGAINST GBV-B CORE AND NS3 PROTEINS BY ELISA

Tamarin and marmoset plasma samples were evaluated for anti-GBV-B core and NS3 antibodies by ELISA as described previously (Ishii et al., 2007).

HISTOPATHOLOGICAL AND IMMUNOHISTOCHEMICAL ANALYSES

Liver samples obtained by necropsy from the GBV-B-infected marmoset were examined histopathologically as previously described (Ishii et al., 2007). For standard histological examination, the sections were subjected to hematoxylin and eosin (HE) staining. Masson's trichrome staining was also performed to estimate the development of fibrosis according to a standard laboratory protocol. To detect the viral protein in tissues, we employed a mouse anti-core monoclonal antibody, 5A10, that we generated. In brief, Mice were immunized with the GBV-B core protein expressed in *E. coli* (Ishii et al., 2007). Hybridoma cells producing an anti-core mAb were screened by both the core-expressing 293T cells and the liver sections of an acutely GBV-B-infected tamarin. Liver samples were fixed in 10% neutral buffered formalin and embedded in paraffin wax. Sections were deparaffinized by pretreating with 0.5% periodic acid and then subjected to antigen retrieval with citric acid buffer and heating in an autoclave for 10 min at 121°C. The sections were then incubated free floating in primary antibody solution (5A10; 1:50 dilution) overnight at 4°C. Following brief washes with wash buffer, the sections were sequentially incubated with a biotinylated goat anti-mouse IgG (1:400 dilution), followed by addition of a streptavidin–biotin–horseradish peroxidase complex (sABC kit; DAKO, Denmark). Immunoreactive elements in the sections were visualized by treatment with 3,3′-diaminobenzidine tetroxide (Dojin Kagaku, Japan), together with counterstaining with hematoxylin.

DETERMINATION OF THE GBV-B SEQUENCE

Viral RNA was isolated from the plasma of GBV-B-infected marmosets as described above. GBV-B cDNA was synthesized using SuperScript reverse transcriptase III (Invitrogen) with random hexamer primers (Invitrogen). The resulting cDNAs were used to obtain PCR amplification products of lengths of 0.5–1.0 kb, using GBV-B-specific primers and LA-Taq DNA polymerase (TaKaRa). The PCR products were then purified from the gel using a QIA-quick gel extraction kit (QIAGEN), and the purified amplimers were sequenced directly using a CEQ-2000XL analysis system (Beckman) with a DTCS quick start kit and GBV-B-specific primers according to the manufacturer's instructions. Sequence data were analyzed using the Sequencher 4.8 (Gene Codes) and Mac Vector 10.6 (MacVector) software packages. The GenBank accession numbers of the viral genome sequences in each time point are as follows: AB630358, AB630359, and AB630360 for 45, 104, and 135 weeks after infection in Cj05-002; AB630361, AB630362, AB630363, and AB630364 for 33, 88, 141, and 229 weeks after infection in Cj05-004, respectively. Throughout this article, the amino acids are numbered according to the full-length genome sequence of isolate pGBB (GenBank accession number AF179612).

RESULTS

GBV-B INFECTION IN TAMARINS AND MARMOSETS

Four tamarins and four marmosets were intrahepatically inoculated with GBV-B and the growth kinetics and pathogenesis of the virus were compared. In tamarins, the peak viral loads in plasma reached 10^9–10^{10} copies/ml in the acute phase and the viremia was maintained for an average of 3 months in parallel with increases in plasma ALT levels (**Figure 1A**). Antibodies reactive with the viral core and NS3 proteins were developed in all of the tamarins as the plasma viral loads were reduced and the antibody titers reached maximum levels concurrently with the complete loss of detectable viral RNA (**Figure 1A**). In contrast, two of four marmosets infected with GBV-B developed chronic infection while the others exhibited a phenotype similar to that of the tamarins (i.e., subacute clearance of the viremia followed by antibody responses). One exception is that lower plasma viral loads (10^7–10^8 copies/ml) were observed in the marmosets relative to those of the tamarins (**Figure 1B**). The details of the chronically infected marmosets are described below.

Case 1: Cj05-002 (**Figures 1B** and **2**). The viral RNA was undetectable until week 4 post infection (p.i.) and then gradually increased to a peak at week 18 p.i. (3×10^7 copies/ml). Subsequently, this case retained intermittent viremia during the observation period of week 180 p.i., while the intervals between the viremia phases were prolonged. Importantly, the titers of anti-core and anti-NS3 antibodies reached a persistent plateau at 6 months and 1 year p.i., respectively. In addition, ALT levels were recurrently increased without observation of other clinical symptoms.

Case 2: Cj05-004 (**Figures 1B** and **2**). During the acute phase of infection, the level of viremia was relatively low and transient, followed by a 1-year period when the virus was essentially undetectable. Irrespective of the very low viral load, the titer of anti-NS3 but not anti-core antibody steadily increased and reached a plateau at week 42 p.i. Moreover, an occasional but obvious increase in the level of ALT was observed during this period. We thus suspected that antigenic stimulation by a lower level of viral growth in the liver, which remained below detectable levels in blood, might lead to the induction of the anti-NS3 antibody and the recurrent ALT increase. Subsequently, viremia became detectable at week 58 p.i. and 10^4–10^5 copies/ml of the viral RNA persisted until week 108 p.i. Thereafter, an abrupt increase of the anti-core antibody was detected, concomitant with augmentation of the viral load of $10^{5.5}$ copies/ml on average and recurrent increases in the ALT level. Eventually, the individual was euthanized at week 229 p.i. because of poor prognosis since the ALT value drastically increased by 161-fold, which was accompanied by a dramatic decrease of platelet counts and a deteriorating general status. Histopathological analyses of the necropsy samples demonstrated that the liver developed diffuse piecemeal necrosis with infiltration of lymphocytes and

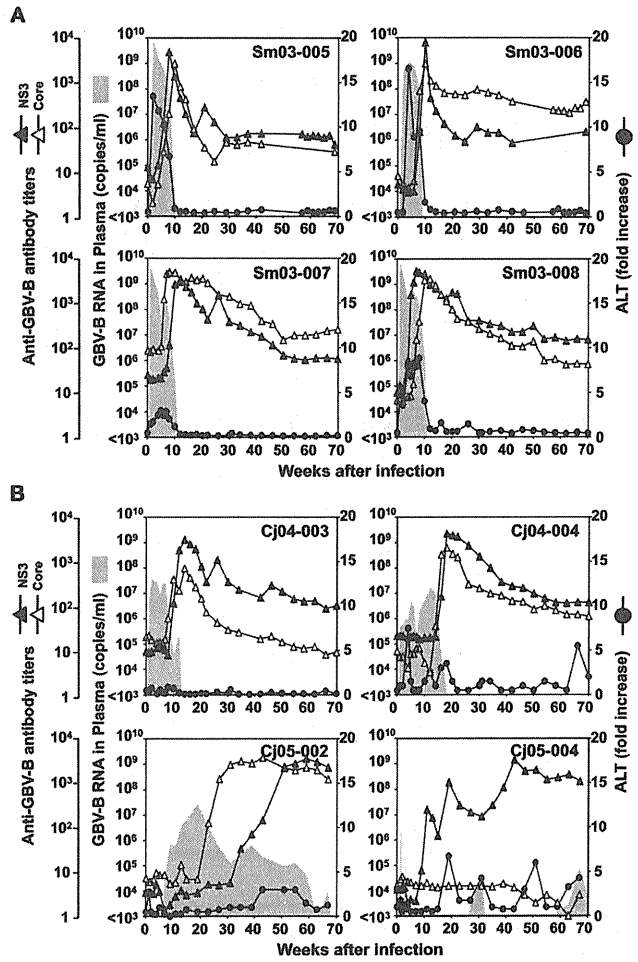

FIGURE 1 | Infection profiles until week 70 p.i. of tamarins (A) and marmosets (B) inoculated intrahepatically with GBV-B infectious serum obtained from a tamarin. Plasma samples periodically obtained from the monkeys were evaluated for the copy numbers of GBV-B genomic RNA (green shaded area), ALT levels (red circles), and the antibody titers against GBV-B core and NS3 (blue and yellow triangles, respectively).

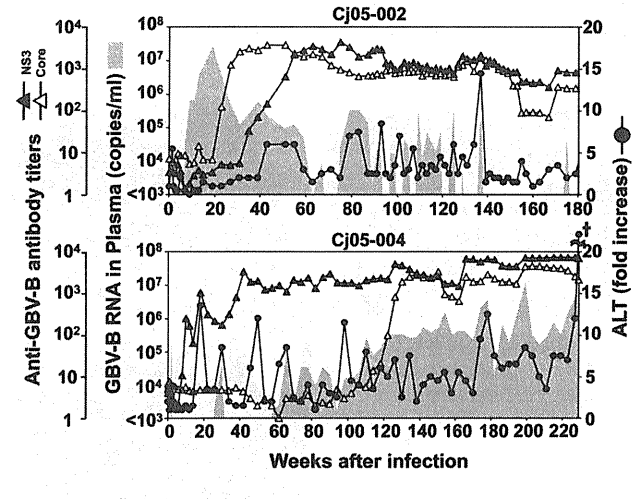

FIGURE 2 | Profiles of the marmosets persistently infected with GBV-B. Plasma samples periodically obtained from the marmosets were evaluated for the copy numbers of GBV-B genomic RNA (green shaded area), ALT levels (red circles), and the antibody titers against GBV-B core and NS3 (blue and yellow triangles, respectively). The cruciate mark in Cj05-004 indicates that the individual was euthanized due to a poor prognosis at week 229 p.i. At that time, the ALT value in plasma had increased by 161-fold.

formation of lymphoid follicles (**Figure 3A**, Appendix). The viral load in the liver was relatively high (3.8×10^4 copies/mg tissue weight), which was similar to the viral load observed for tamarins acutely infected with GBV-B (Ishii et al., 2007). The high viral load in the liver was consistent with a large number of granular positive signals for the core protein, which was in similar manner with the core protein of HCV (Miyanari et al., 2007), as immunostained with an anti-GBV-B core monoclonal antibody (**Figure 3B**). Notably, Masson trichrome staining (**Figures 3C,D**) as well as Elastica van Gieson staining (Appendix) demonstrated that the liver also developed diffuse and abundant fibrosis. The disease of this marmoset was therefore diagnosed as a case of acute exacerbation of progressive chronic hepatitis by GBV-B infection.

ANALYSIS OF MUTATIONS IN GBV-B GENOMES

Next, we determined the dominant sequence of the viral genomes at weeks 45, 104, and 135 p.i. in Cj05-002 and weeks 33, 88, 141, and 229 p.i. in Cj05-004. As seen in **Figure 4A**, it was found that there was no specific region in which extensive nucleotide mutations occurred throughout the study periods and that the nucleotide mutation rates were $1.9–2.9 \times 10^{-3}$ and $1.5–3.6 \times 10^{-3}$ changes per site per year in Cj05-002 and Cj05-004, respectively (**Table 1**). In terms of amino acid substitution, we observed the following: (i) several back or sequential mutations (G250V > A, S731L > S, E2346G > E in Cj05-002; V254A > V, I285V > I, L495S > L, T735A > T, F2135L > F > S in Cj05-004) in both marmosets; (ii) highly selective non-synonymous mutations that were remarkable in E1, but such mutations were rarely observed in core (**Figures 4** and **5**); and (iii) the non-synonymous mutation rates were $1.8–4.0 \times 10^{-3}$ and $2.1–4.6 \times 10^{-3}$ substitutions per site per year in Cj05-002 and Cj05-004, respectively (**Figures 4** and **5**; **Table 2**). (iv) The non-synonymous changes detected mainly in NS5A and NS5B in both animals were also observed in a number of previous reports (Simons et al., 1995; Bukh et al., 1999; Sbardellati et al., 2001; Martin et al., 2003; Nam et al., 2004; Kyuregyan et al., 2005; Weatherford et al., 2009; Takikawa et al., 2010). It may be reasonable to consider that the molecular clone we employed (Bukh et al., 1999) was derived from a minor clone of mixed populations and emergence of a new mutations easily occurred as a mechanism of GBV-B adaptation to a new host, while it is also possible that "consensus" non-synonymous changes were due to either a result of a selection of the pre-existent minor variants. Taken together, these results suggest that efficient

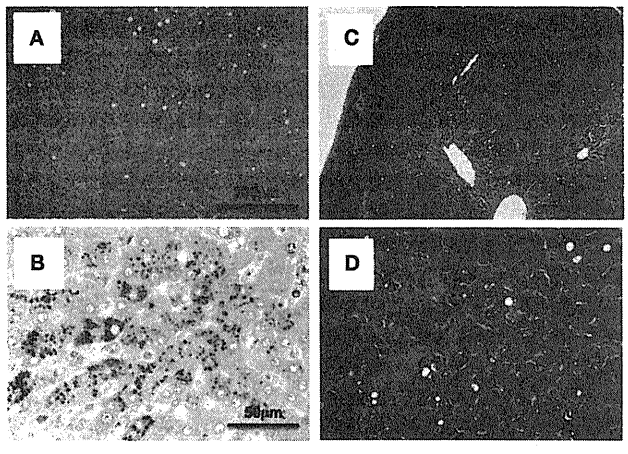

FIGURE 3 | Histopathological and immunohistochemical analyses of the liver from Cj05-004 at week 229 p.i. HE staining (A), immunohistochemical staining for the core protein of GBV-B (B), and Masson's trichrome staining (C,D) are shown.

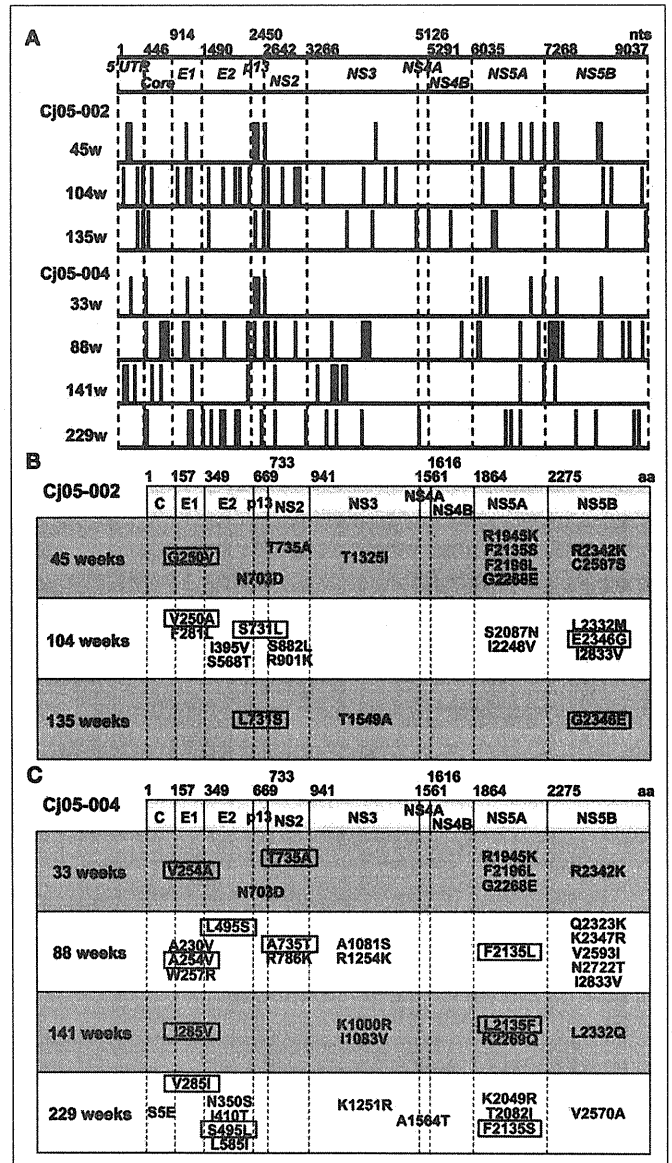

FIGURE 4 | Mutations in the viral genome sequences amplified from plasma of the marmosets persistently infected with GBV-B. (A) Positions of the nucleotide mutations in the viral genome sequences at multiple time points (at weeks 45, 104, and 135 in Cj05-002 and weeks 33, 88, 141, and 229 in Cj05-004) are illustrated as bars. **(B,C)** Positions of the non-synonymous mutations in the viral genome sequences at multiple time points are shown. **(B)** Cj05-002; **(C)** Cj05-004. Positions of the mutations that had been identified in previous reports are indicated as black, while those unidentified previously are shown as blue. Red squares illustrate back or sequential mutations.

Table 1 | Summary of the nucleotide substitutions in GBV-B genome sequences amplified from plasma of the marmosets persistently infected with GBV-B.

Genomic region	nt position	No. (%) of nt differences						
		Cj05-002			Cj05-004			
		45 weeks	104 weeks	135 weeks	33 weeks	88 weeks	141 weeks	229 weeks
5′UTR	1–445	2 (0.45)	3 (0.67)	2 (0.45)	1 (0.22)	0 (0)	3 (0.67)	0 (0)
Core	446–913	0 (0)	1 (0.21)	1 (0.21)	1 (0.21)	4 (0.85)	2 (0.43)	3 (0.64)
E1	914–1489	1 (0.17)	3 (0.52)	0 (0)	1 (0.17)	3 (0.52)	1 (0.17)	2 (0.35)
E2	1490–2449	0 (0)	5 (0.52)	1 (0.10)	0 (0)	2 (0.21)	1 (0.10)	6 (0.63)
p13	2450–2641	2 (1.04)	1 (0.52)	2 (1.04)	2 (1.04)	1 (0.52)	0 (0)	1 (0.52)
NS2	2642–3265	1 (0.16)	5 (0.80)	1 (0.16)	1 (0.16)	4 (0.64)	1 (0.16)	2 (0.32)
NS3	3266–5125	1 (0.05)	4 (0.22)	3 (0.16)	0 (0)	5 (0.27)	6 (0.32)	3 (0.16)
NS4A	5126–5290	0 (0)	0 (0)	0 (0)	0 (0)	0 (0)	0 (0)	1 (0.61)
NS4B	5291–6034	0 (0)	0 (0)	2 (0.27)	0 (0)	1 (0.13)	0 (0)	0 (0)
NS5A	6035–7267	6 (0.49)	4 (0.32)	2 (0.16)	4 (0.32)	4 (0.32)	2 (0.16)	3 (0.24)
NS5B	7268–9037	4 (0.23)	5 (0.28)	3 (0.17)	2 (0.11)	10 (0.56)	1 (0.06)	4 (0.23)
Total	9037	17 (0.19)	31 (0.34)	17 (0.19)	12 (0.13)	34 (0.38)	17 (0.19)	25 (0.28)
Mutation rate/year		2.2×10^{-3}	3.0×10^{-3}	3.2×10^{-3}	2.1×10^{-3}	3.6×10^{-3}	1.8×10^{-3}	1.6×10^{-3}

Table 2 | Summary of the amino acid substitutions in GBV-B genome sequences amplified from plasma of the marmosets persistently infected with GBV-B.

Amino acid region	aa position	No. (%) of aa differences						
		Cj05-002			Cj05-004			
		45 weeks	104 weeks	135 weeks	33 weeks	88 weeks	141 weeks	229 weeks
Core	1–156	0 (0)	0 (0)	0 (0)	0 (0)	0 (0)	0 (0)	1 (0.64)
E1	157–348	1 (0.52)	2 (1.04)	0 (0)	1 (0.52)	3 (1.56)	1 (0.52)	1 (0.52)
E2	349–613	0 (0)	2 (0.63)	0 (0)	0 (0)	1 (0.31)	0 (0)	4 (1.25)
P13	669–732	1 (1.56)	1 (1.56)	1 (1.56)	1 (1.56)	0 (0)	0 (0)	0 (0)
NS2	733–940	1 (0.48)	2 (0.96)	0 (0)	1 (0.48)	2 (0.96)	0 (0)	0 (0)
NS3	941–1560	1 (0.16)	0 (0)	1 (0.16)	0 (0)	2 (0.32)	2 (0.32)	1 (0.16)
NS4A	1561–1615	0 (0)	0 (0)	0 (0)	0 (0)	0 (0)	0 (0)	1 (1.82)
NS4B	1616–1863	0 (0)	0 (0)	0 (0)	0 (0)	0 (0)	0 (0)	0 (0)
NS5A	1864–2274	4 (0.97)	2 (0.49)	0 (0)	3 (0.73)	1 (0.24)	2 (0.49)	3 (0.73)
NS5B	2275–2864	2 (0.34)	3 (0.51)	1 (0.17)	1 (0.17)	5 (0.85)	1 (0.17)	1 (0.17)
Total	2864	10 (0.38)	12 (0.42)	3 (0.10)	7 (0.24)	14 (0.49)	6 (0.21)	12 (0.42)
Mutation rate/year		4.0×10^{-3}	3.7×10^{-3}	1.8×10^{-3}	3.9×10^{-3}	4.6×10^{-3}	2.1×10^{-3}	2.5×10^{-3}

and selective evasion from immune pressure in the two marmosets resulted in long-term persistent GBV-B infection accompanied by subsequent chronic hepatitis.

DISCUSSION

In this study, we show for the first time that GBV-B is capable of eliciting a chronic and progressive hepatitis C-like disease in marmosets. Evidence for this condition is demonstrated by long-term persistent GBV-B infection, recurrent ALT increase, and fibrosis. Moreover, one of the chronically infected marmosets developed acute exacerbation of chronic hepatitis as indicated by diffuse piecemeal liver necrosis and an ALT flare, which is seen in patients with viral hepatitis (Perrillo, 1997). While the usefulness of the monkey model as a surrogate model for HCV infection has been under debate due to the virtual inability of GBV-B to cause chronic hepatitis C-like disease in tamarins, the present data demonstrate that the ability of GBV-B to induce the chronic disease is likely to be inherent depending on the differences between species and individuals.

It has been reported that tamarins generally permit extensive replication of GBV-B in the subacute phase of infection and develop acute hepatitis as shown by significant increases of serum enzymes such as ALT and isocitrate dehydrogenase. The viral load in marmosets seems to be lower than in tamarins (Lanford et al.,

2003; Bright et al., 2004; Woollard et al., 2008; Weatherford et al., 2009). A recent report indicated that marmosets exhibit susceptible and partially resistant phenotypes upon infection with GBV-B (Weatherford et al., 2009). Consistent with this finding, the present results also showed that the marmosets appeared to exhibit two phenotypes (**Figure 1B**). Importantly, the long-term persistent GBV-B infection was established in the marmosets with lower viral loads during the initial weeks p.i. (**Figure 1B**; Cj05-002 and Cj05-004). This suggests that the mild viral growth in the marmosets with a "partially resistant" phenotype is critical for the establishment of the chronic infection. Of note, the viral growth was undetectable until week 6 p.i. in Cj05-002, owing to unexpected interferon responses that were induced by administration of an anti-luciferase small interfering RNA in a cationic liposome formulation 2 days before GBV-B infection (Yokota et al., 2007). Irrespective of the partial suppression of the viral growth, humoral immune responses were delayed and consequently the individual developed chronic infection. Taken together, it is reasonable to assume that the viral persistence in marmosets may be closely associated with inefficient antiviral immune responses that are elicited at the periods of the lower viral loads. Previously, we and others employed relatively higher amounts of GBV-B for challenge in tamarins and marmosets. This could result in greater viral loads in the acute phase than those in humans and chimpanzees infected with HCV, followed by induction of efficient protective immunity and acute clearance. To clarify the mechanisms by which chronic GBV-B infection is established, further characterization of the differences in innate and acquired antiviral immunity between individuals with acute clearance and chronic infection will be needed.

Accumulating evidence suggests that escape mutations occurring during the course of chronic HCV infection may lead to evasion of humoral and cellular antiviral immunity (Bowen and Walker, 2005a,b; Burke and Cox, 2010). Consistent with these observations, we found that GBV-B acquired multiple back or sequential non-synonymous mutations (e.g., G250V > A, S731L > S, E2346G > E in Cj05-002; and V254A > V, I285V > I, L495S > L, T735A > T, F2135L > F > S in Cj05-004) in the chronically infected marmosets. Highly selective non-synonymous mutations were identified especially in E1, but such mutations were rarely observed in core (**Figures 4** and **5**). Moreover, the non-synonymous mutations in the E1 and NS3 regions occurred throughout the observation periods in Cj05-004 with chronic GBV-B infection, which had not been identified previously (Simons et al., 1995; Bukh et al., 1999; Sbardellati et al., 2001; Martin et al., 2003; Nam et al., 2004; Kyuregyan et al., 2005; Weatherford et al., 2009; Takikawa et al., 2010). Together with the finding that the rates of both synonymous and non-synonymous mutations were similar to those observed in cases of HCV (Ogata et al., 1991; Fernandez et al., 2004), these results strongly suggest that efficient and selective evasion from immune pressures may result in long-term persistent GBV-B infection and subsequent chronic hepatitis. Further analyses on the functional significance of the non-synonymous mutations will clarify this possibility.

It is surprising that in Cj05-004, the antibody titer to NS3 was observed to steadily increase after week 10 p.i. irrespective of the scarce viral loads over 1 year p.i., including the bipartite

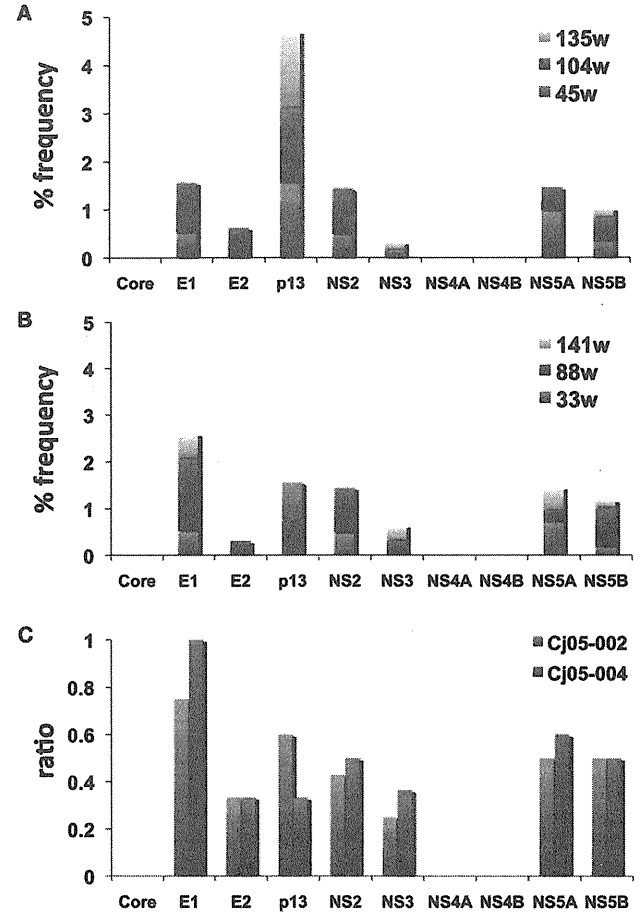

FIGURE 5 | The frequency of the non-synonymous mutations in the viral genome sequences amplified from plasma of the marmosets persistently infected with GBV-B. (A,B) The accumulated frequency of the non-synonymous mutations per total amino acid numbers of each viral protein at multiple time points are illustrated [**(A)** at weeks 45, 104, and 135 in Cj05-002; **(B)** weeks 33, 88, and 141 in Cj05-004]. To compare the frequency between the two marmosets, the data at week 229 p.i. in Cj05-004 are omitted. **(C)** The ratio of the non-synonymous mutations per total numbers of nucleotide mutations identified at weeks 45, 104, and 135 in Cj05-002 and at weeks 33, 88, and 141 in Cj05-004 in each viral gene. To compare the frequency between the two marmosets, the data at week 229 p.i. in Cj05-004 are omitted.

periods of weeks 4–26 and 34–58 p.i. when the virus was undetectable (**Figure 1**). Considering that three spikes of ALT levels were observed during these periods, our results suggest that antigenic stimulation by the lower level of viral growth in the liver, which was below detectable levels in blood, may induce the antibody and cytotoxic T-cell responses. In addition, during longitudinal analyses of monkeys experimentally infected with GBV-B, it is important to comprehensively evaluate multiple parameters, including viral loads, serum enzymes, and antibodies against core and NS3 proteins, to define whether virus-infected monkeys that produce no detectable viremia for a period of time have cleared the virus or are experiencing a latent period of chronic infection.

ACKNOWLEDGMENTS

We wish to thank T. Kurosawa, M. Fujita, and T. Ikoma for their helpful assistance and the members of Corporation for Production and Research of Laboratory Primates for technical assistance. Financial support: This work was supported by grants from the Ministry of Health, Labor, and Welfare of Japan (to Hirofumi Akari).

REFERENCES

Akari, H., Iwasaki, Y., Yoshida, T., and Iijima, S. (2009). Non-human primate surrogate model of hepatitis C virus infection. *Microbiol. Immunol.* 53, 53–57.

Beames, B., Chavez, D., Guerra, B., Notvall, L., Brasky, K. M., and Lanford, R. E. (2000). Development of a primary tamarin hepatocyte culture system for GB virus-B: a surrogate model for hepatitis C virus. *J. Virol.* 74, 11764–11772.

Beames, B., Chavez, D., and Lanford, R. E. (2001). GB virus B as a model for hepatitis C virus. *ILAR J.* 42, 152–160.

Boonstra, A., van der Laan, L. J., Vanwolleghem, T., and Janssen, H. L. (2009). Experimental models for hepatitis C viral infection. *Hepatology* 50, 1646–1655.

Bowen, D. G., and Walker, C. M. (2005a). Mutational escape from CD8+ T cell immunity: HCV evolution, from chimpanzees to man. *J. Exp. Med.* 201, 1709–1714.

Bowen, D. G., and Walker, C. M. (2005b). Adaptive immune responses in acute and chronic hepatitis C virus infection. *Nature* 436, 946–952.

Bright, H., Carroll, A. R., Watts, P. A., and Fenton, R. J. (2004). Development of a GB virus B marmoset model and its validation with a novel series of hepatitis C virus NS3 protease inhibitors. *J. Virol.* 78, 2062–2071.

Bukh, J. (2004). A critical role for chimpanzee model in the study of hepatitis C. *Hepatology* 39, 1469–1475.

Bukh, J., Apgar, C. L., and Yanagi, M. (1999). Toward a surrogate model for hepatitis C virus: An infectious molecular clone of the GB virus-B hepatitis agent. *Virology* 262, 470–478.

Bukh, J., Thimme, R., Meunier, J. C., Faulk, K., Spangenberg, H. C., Chang, K. M., Satterfield, W., Chisari, F. V., and Purcell, R. H. (2008). Previously infected chimpanzees are not consistently protected against reinfection or persistent infection after reexposure to the identical hepatitis C virus strain. *J. Virol.* 82, 8183–8195.

Burke, K. P., and Cox, A. L. (2010). Hepatitis C virus evasion of adaptive immune responses: a model for viral persistence. *Immunol. Res.* 47, 216–227.

Chisari, F. V. (2005). Unscrambling hepatitis C virus-host interactions. *Nature* 436, 930–932.

Feld, J. J., and Hoofnagle, J. H. (2005). Mechanism of action of interferon and ribavirin in treatment of hepatitis C. *Nature* 436, 967–972.

Fernandez, J., Taylor, D., Morhardt, D. R., Mihalik, K., Puig, M., Rice, C. M., Feinstone, S. M., and Major, M. E. (2004). Long-term persistence of infection in chimpanzees inoculated with an infectious hepatitis C virus clone is associated with a decrease in the viral amino acid substitution rate and low levels of heterogeneity. *J. Virol.* 78, 9782–9789.

Hoofnagle, J. H. (1997). Hepatitis C: the clinical spectrum of disease. *Hepatology* 26, 15S–20S.

Ishii, K., Iijima, S., Kimura, N., Lee, Y. J., Ageyama, N., Yagi, S., Yamaguchi, K., Maki, N., Mori, K., Yoshizaki, S, Machida, S., Suzuki, T., Iwata, N., Sata, T., Terao, K., Miyamura, T., and Akari, H. (2007). GBV-B as a pleiotropic virus: distribution of GBV-B in extrahepatic tissues in vivo. *Microbes Infect.* 9, 515–521.

Jacob, J. R., Lin, K. C., Tennant, B. C., and Mansfield, K. G. (2004). GB virus B infection of the common marmoset (*Callithrix jacchus*) and associated liver pathology. *J. Gen. Virol.* 85, 2525–2533.

Kyuregyan, K. K., Poleschuk, V. F., Zamyatina, N. A., Isaeva, O. V., Michailov, M. I., Ross, S., Bukh, J., Roggendorf, M., and Viazov, S. (2005). Acute GB virus B infection of marmosets is accompanied by mutations in the NS5A protein. *Virus Res.* 114, 154–157.

Lanford, R. E., Chavez, D., Notvall, L., and Brasky, K. M. (2003). Comparison of tamarins and marmosets as hosts for GBV-B infections and the effect of immunosuppression on duration of viremia. *Virology* 311, 72–80.

Lavanchy, D. (2009). The global burden of hepatitis C. *Liver Int.* 29, 74–81.

Martin, A., Bodola, F., Sanger, D. V., Goettge, K., Popov, V., Rijnbrand, R., Lanford, R. E., and Lemon, S. M. (2003). Chronic hepatitis associated with GB virus B persistence in a tamarin after intrahepatic inoculation of synthetic viral RNA. *Proc. Natl. Acad. Sci. U.S.A.* 100, 9962–9967.

Melnikova, I. (2008). Hepatitis C therapies. *Nat. Rev. Immunol.* 5, 799–800.

Miyanari, Y., Atsuzawa, K., Usuda, N., Watashi, K., Hishiki, T., Zayas, M., Bartenschlager, R., Wakita, T., Hijikata, M., and Shimotohno, K. (2007). The lipid droplet is an important organelle for hepatitis C virus production. *Nat. Cell Biol.* 9, 1089–1097.

Muerhoff, A. S., Leary, T. P., Simons, J. N., Pilot-Matias, T. J., Dawson, G. J., Erker, J. C., Chalmers, M. L., Schlauder, G. G., Desai, S. M., and Mushahwer, I. K. (1995). Genomic organization of GB viruses A and B: two new members of the Flaviviridae associated with GB agent hepatitis. *J. Virol.* 69, 5621–5630.

Nam, J. H., Faulk, K., Engle, R. E., Govindarajan, S., St. Claire, M., and Bukh, J. (2004). In vivo analysis of the 3′ untranslated region of GB virus B after in vitro mutagenesis of an infections cDNA clone: persistent infection in a transfected tamarin. *J. Virol.* 78, 9389–9399.

Ogata, N., Alter, H. J., Miller, R. H., and Purcell, R. H. (1991). Nucleotide sequence and mutation rate of the H strain of hepatitis C virus. *Proc. Natl. Acad. Sci. U.S.A.* 88, 3392–3396.

Ohba, K., Mizokami, M., Lau, J. Y., Orito, E., Ikeo, K., and Gojobori, T. (1996). Evolutionary relationship of hepatitis C, pesti-, flavi-, plantviruses, and newly discovered GB hepatitis agents. *FEBS Lett.* 378, 232–234.

Perrillo, R. P. (1997). The role of liver biopsy in hepatitis C. *Hepatology* 26, 57S–61S.

Rehermann, B., and Nascimbeni, M. (2005). Immunology of hepatitis B virus and hepatitis C virus infection. *Nat. Rev. Immunol.* 5, 215–229.

Sbardellati, A., Scarselli, E., Verschoor, E., De Tomassi, A., Lazzaro, D., and Traboni, C. (2001). Generation of infectious and transmissible virions from a GB virus B full-length consensus clone in tamarins. *J. Gen. Virol.* 82, 2437–2448.

Seeff, L. B., and Hoofnagle, J. H. (2002). National Institutes of Health Consensus Development Conference: management of hepatitis C: 2002. *Hepatology* 36, S1–S2.

Simons, J. N., Pilot-Matias, T. J., Leary, T. P., Dawason, G. J., Desai, S. M., Schlauder, G. G., Muerhoff, A. S., Erker, J. C., Buijk, S. L., Chalmers, M. L., Van Sant, C. L., and Mushahwar, I. K. (1995). Identification of two *Flavivirus*-like genomes in the GB hepatitis agent. *Proc. Natl. Acad. Sci. U.S.A.* 92, 3401–3405.

Takikawa, S., Engle, R. E., Faulk, K. N., Emerson, S. U., Purcell, R. H., and Bukh, J. (2010). Molecular evolution of GB virus B hepatitis virus during acute resolving and persistent infections in experimentally infected tamarins. *J. Gen. Virol.* 91, 727–733.

Weatherford, T., Chavez, D., Brasky, K. M., and Lanford, R. E. (2009). The marmoset model of GB virus B infections: adaptation to host phenotypic variation. *J. Virol.* 83, 5806–5814.

Woollard, D. J., Haqshenas, G., Dong, X., Pratt, B. F., Kent, S. J., and Gowans, E. J. (2008). Virus-specific T-cell immunity correlates with control of GB virus B infection in marmosets. *J. Virol.* 82, 3054–3060.

Yokota, T., Iijima, S., Kubodera, T., Ishii, K., Katakai, Y., Ageyama, N., Chen, Y., Lee, Y. J., Unno, T., Nishina, K., Iwasaki, Y., Maki, N., Mizusawa, H., and Akari, H. (2007). Efficient regulation of viral replication by siRNA in a non-human primate surrogate model for hepatitis C. *Biochem. Biophys. Res. Commun.* 361, 294–300.

Conflict of Interest Statement: The authors declare that the research was conducted in the absence of any commercial or financial relationships that could be construed as a potential conflict of interest.

Received: 21 October 2011; paper pending published: 31 October 2011; accepted: 15 November 2011; published online: 07 December 2011.

Citation: Iwasaki Y, Mori K-i, Ishii K, Maki N, Iijima S, Yoshida T, Okabayashi S, Katakai Y, Lee Y-J, Saito A, Fukai H, Kimura N, Ageyama N, Yoshizaki S, Suzuki T, Yasutomi Y, Miyamura T, Kannagi M and Akari H (2011) Long-term persistent GBV-B infection and development of a chronic and progressive hepatitis C-like disease in marmosets. Front. Microbio. 2:240. doi: 10.3389/fmicb.2011.00240

This article was submitted to Frontiers in Virology, a specialty of Frontiers in Microbiology.

APPENDIX

MATERIALS AND METHODS

Liver samples obtained by necropsy from the GBV-B-infected marmosets were histopathologically analyzed as described in Section "Materials and Methods." Elastica–van Gieson staining was performed to evaluate fibrosis according to a standard laboratory protocol. To detect CD3 and CD20 antigens, liver samples were fixed in 10% neutral buffered formalin and embedded in paraffin wax. Sections were deparaffinized by pretreatment with 0.5% periodic acid and then subjected to antigen retrieval with citric acid buffer and heating in an autoclave for 10 min at 121°C. Sections were then incubated free floating in the monoclonal antibody solution for CD20 (DAKO) and CD3 (DAKO) overnight at 4°C. Following brief washes with buffer, the sections were sequentially incubated with biotinylated goat anti-mouse IgG (1:400), followed by streptavidin–biotin–horseradish peroxidase complex (sABC kit; DAKO, Denmark). Immunoreactive elements were visualized by treating the sections with 3,3′-diaminobenzidine tetroxide (Dojin Kagaku, Japan). The sections were then counterstained with hematoxylin.

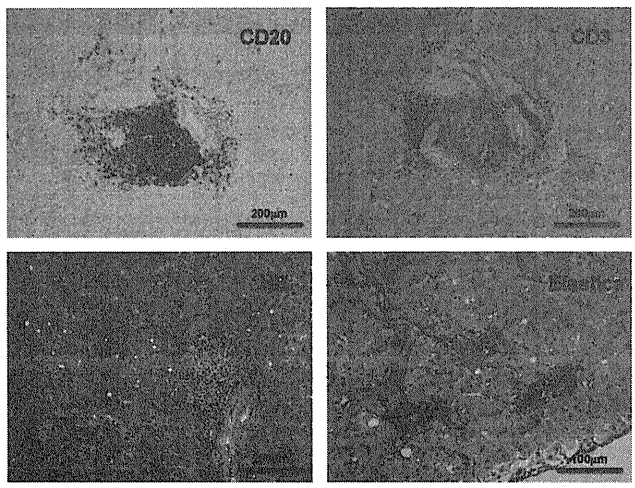

FIGURE A1 | Histopathological and immunohistochemical analyses of the liver from Cj05-004 at week 229 p.i.

Reduced Replication Capacity of NL4-3 Recombinant Viruses Encoding Reverse Transcriptase–Integrase Sequences From HIV-1 Elite Controllers

Zabrina L. Brumme, PhD,†‡ Chun Li, BSc,‡§ Toshiyuki Miura, MD,‡‖ Jennifer Sela, BSc,‡ Pamela C. Rosato, BSc,‡ Chanson J. Brumme, BSc,†‡ Tristan J. Markle, BSc,* Eric Martin, BSc,*§§ Brian L. Block, BSc,‡ Alicja Trocha, DVM,‡ Carl M. Kadie, PhD,¶ Todd M. Allen, PhD,‡ Florencia Pereyra, MD,‡ David Heckerman, MD, PhD,¶ Bruce D. Walker, MD,‡# and Mark A. Brockman, PhD*§§†‡*

Background: Identifying viral and host determinants of HIV-1 elite control may help inform novel therapeutic and/or vaccination strategies. Previously, we observed decreased replication capacity in controller-derived viruses suggesting that fitness consequences of human leukocyte antigen (HLA) class I–associated escape mutations in Gag may contribute to this phenotype. This study examines whether similar functional defects occur in Pol proteins of elite controllers.

Methods: Recombinant NL4-3 viruses encoding plasma RNA-derived reverse transcriptase–integrase sequences from 58 elite controllers and 50 untreated chronic progressors were constructed, and replication capacity measured in vitro using a green fluorescent protein (GFP) reporter T-cell assay. Sequences were analyzed for drug resistance and HLA-associated viral polymorphisms.

Results: Controller-derived viruses displayed significantly lower replication capacity compared with those from progressors ($P < 0.0001$). Among controllers, the most attenuated viruses were generated from individuals expressing HLA-B*57 or B*51. In viruses from B*57+ progressors (n = 8), a significant inverse correlation was observed between B*57-associated reverse transcriptase–integrase escape mutations and replication capacity ($R = -0.89$; $P = 0.003$); a similar trend was observed in B*57+ controller-derived viruses (n = 20, $R = -0.36$; $P = 0.08$).

Conclusions: HIV-1 Pol function seemed to be compromised in elite controllers. As observed previously for Gag, HLA-associated immune pressure in Pol may contribute to viral attenuation and subsequent control of viremia.

Key Words: Cytotoxic T-lymphocyte, elite controller, HIV-1, HLA class I, immune escape, Pol, viral replication capacity

(*J Acquir Immune Defic Syndr* 2011;56:100–108)

INTRODUCTION

Elite controllers are a rare group of HIV-1–infected individuals who spontaneously maintain plasma viremia below the limit of standard clinical detection (<50 viral RNA copies/mL) without antiviral therapy.[1] Elucidating the mechanisms responsible for this phenotype may reveal host and viral factors that may be modulated for prophylactic or therapeutic intervention.

HIV-1 replication capacity (RC) likely plays an important role in pathogenesis,[2,3] but its relevance to the elite controller phenotype remains unclear. Although a recent examination of a large number of elite controller-derived HIV sequences revealed no evidence of gross mutational defects, large insertions or deletions, nor shared ancestry,[4] virus function may nevertheless be compromised. Indeed, previous studies have reported lower RC in viruses isolated from viremic long-term nonprogressors compared with those from

Received for publication January 5, 2010; accepted September 23, 2010.

From the *Faculty of Health Sciences and §§Department of Molecular Biology and Biochemistry, Simon Fraser University, Burnaby BC, Canada; †British Columbia Centre for Excellence in HIV/AIDS, Vancouver BC, Canada; ‡Ragon Institute of MGH, MIT, and Harvard, Boston, MA; §Program of Biological Sciences in Dental Medicine, Harvard University, Cambridge, MA; ‖Division of Infectious Diseases Advanced Clinical Research Center, Institute of Medical Science, University of Tokyo, Tokyo, Japan; ¶Microsoft Research, Redmond WA; and #Howard Hughes Medical Institute, Chevy Chase, MD.

Supported in part by grants AI028568 and AI030914 from the NIAID-NIH, the Howard Hughes Medical Institute, the Harvard University Center for AIDS Research, the Bill and Melinda Gates Foundation, and a gift from the Mark and Lisa Schwartz Foundation (to B.D.W.), and an Operating Grant from the Canadian Institutes of Health Research (CIHR) and a Jim Gray Seed Grant from Microsoft Research (to M.A.B. and Z.L.B.). Z.L.B. is supported by a CIHR New Investigator Award. C.J.B. is supported by a NSERC Julie Payette Scholarship.

Presented in part as: Li C, Brumme ZL, Miura T, Rosato P, Sela J, Brumme CJ, Heckerman D, Pereyra F, Walker BD, Brockman MA. Reduced replication capacity of NL4-3 chimeric viruses encoding reverse transcriptase–integrase sequences from HIV-1 elite controllers. AIDS Vaccine. 2009. Abstract P09-11.

The authors Z.L.B., C.L. contributed equally.

The authors declare no conflicts of interest related to this study.

Correspondence to: Mark A. Brockman, PhD, Associate Professor, Molecular Biology and Biochemistry, Simon Fraser University, South Sciences Building, Room 7153, 8888 University Drive, Burnaby, BC, Canada V5A 1S6 (e-mail: mark_brockman@sfu.ca).

Supplemental digital content is available for this article. Direct URL citations appear in the printed text and are provided in the HTML and PDF versions this article on the journal's Web site (www.jaids.com).

chronically infected individuals,[2,3,5] and reduced entry efficiency has been observed for elite controller-derived envelopes compared with those from chronically infected individuals.[6]

Although RC is determined in large part by the founder virus acquired at transmission,[7,8] it can change over time as host and other selective pressures drive intrahost HIV-1 evolution.[9–11] In vitro fitness costs of HLA-restricted cytotoxic T-lymphocyte (CTL) escape mutations in Gag[12–17] and Nef[18] have been demonstrated, and evidence suggests that immune-mediated fitness defects may be relevant to the controller phenotype.[19,20] A recent case report described reduced RC of virus isolated from a B*27/B*57-expressing elite controller compared with the transmitted donor virus.[19] Furthermore, we have previously described reduced in vitro RC of recombinant viruses expressing Gag-Protease from elite controllers compared with progressors in chronic[20] and acute/early[21] infection, an observation attributable at least in part to immune selection.[20,22] A biologically relevant role for immune-mediated fitness defects is supported by relative early viremia control in individuals who acquire HIV-1 harboring escape mutations from donors expressing protective HLA alleles.[7,8] Moreover, evidence for sequential reductions in RC as a result of the accumulation of HLA-restricted CTL escape mutations has been reported in Gag.[16,23]

However, comparably little is known about the consequence of mutations outside of the *Gag* gene on viral RC in elite controllers, and what relevance this may have to the controller phenotype. Because mutations in the *Pol* gene that emerge under antiretroviral drug selection pressures can affect fitness,[24–28] we therefore examined whether elite controller viruses exhibited functional defects in this gene. To do this, recombinant viruses encoding plasma RNA-derived reverse transcriptase (RT)–integrase sequences were generated in an NL4-3 virus backbone from 58 elite controllers and 50 untreated chronic progressors and their in vitro RC was examined using a GFP reporter T-cell assay.[20,29] Similar to previous observations for Gag-Protease[20,21] and Envelope,[6] we observed reduced function of controller-derived RT–integrase, indicating that differences in Pol activity may contribute to HIV-1 control.

METHODS

Study Participants

Fifty-eight elite controllers {all <50 copies RNA/mL; median CD4 = 799 [interquartile range (IQR): 593–1037] cells/mm^3} and 50 untreated chronic progressors [median viral load 4.98 (IQR: 4.51–5.35) $\log_{10}$ copies RNA/ml; median CD4 = 318 (IQR: 61–476) cells/mm^3] were included. Characteristics of this elite controller cohort have been described previously.[30] In addition, 76 of these 108 (70%) patients were previously evaluated for Gag-Protease function.[20] HLA class I typing was performed using standard sequence-based methods. This study was approved by the institutional review board at Massachusetts General Hospital; written informed consent was obtained from all participants.

Generation of Recombinant RT–Integrase Viruses

Bulk (Quasispecies) Method

For elite controllers, reverse transcriptase–polymerase chain reaction (RT-PCR) products spanning Pol were generated as described.[4] For progressors, HIV-1 Pol was RT-PCR amplified from extracted plasma HIV RNA using sequence-specific primers. Second-round polymerase chain reaction (PCR) was performed using PAGE-purified "recombination primers" designed to match the NL4-3 sequence directly upstream of RT (forward; 100bp) and downstream of integrase (reverse; 98bp). Primer sequences are available upon request.

Plasmid pNL4-3ΔRT-Integrase was developed by inserting unique restriction enzyme sites for BstEII at the 5′ end of RT and the 3′ end of integrase using the QuikChange XL kit (Stratagene) followed by deletion of the intervening region by BstEII digestion (New England Biolabs, Ipswich, MA). This plasmid was maintained using Stbl3 E. coli cells (Invitrogen, Burlington, ON, Canada). To generate recombinant viruses, 10 μg of BstEII-linearized plasmid plus 50 μL of second-round amplicon (approximately 5 μg) were mixed with 2.0×10^6 cells of a Tat-driven GFP reporter T-cell line (GXR25 cells[29]) in 800 μL of R10+ medium (RPMI 1640 containing 10% FCS, 2 mM L-glutamine, 100 units/mL penicillin, and 100 μg/mL streptomycin), and transfected by electroporation using a BioRad GenePulser Xcell (exponential protocol: 300V, 500 μF). After transfection, cells were rested for 45 minutes at room temperature, transferred to 25 cm^2 flasks in 5 mL of R10+ medium, and fed with 5 mL R10+ medium on day 5. GFP expression was monitored daily by flow cytometry (FACScalibur, BD Biosciences) starting on day 10. Once GFP+ expression reached ~15% among viable cells, representing the early phase of exponential spread, culture supernatants containing the recombinant viruses were harvested and aliquots stored at −80°C.

Clonal Method

In addition, RT–integrase sequences from a random subset of 14 controllers and 10 progressors were cloned (TOPO-TA cloning kit; Invitrogen, Burlington, ON, Canada), purified and used as starting material to generate recombinant viruses as described above. All clones were resequenced to confirm patient origin.

RC Assays

Virus titers and replication assays were performed as described.[12,20,29] Replication assays were initiated at multiplicity of infection = 0.003, and included 6 negative (uninfected cells only) and 6 NL4-3 controls in each experiment. For each virus, the natural log of the slope of the percent of GFP+ cells was calculated during the exponential phase of viral spread in culture (days 3–6). This value was divided by the mean rate of spread of NL4-3 to generate a normalized, quantitative measure of RC. An RC of 1.0 indicates a rate of spread equal to NL4-3, whereas RC <1.0 and >1.0 indicate rates of spread that are slower than or faster than NL4-3, respectively. All assays were performed in triplicate in

independent experiments, and replication rates were averaged. The experimental procedure is illustrated in the Supplemental Material (see **Figure 1 Supplemental Digital Content 1**, http://links.lww.com/QAI/A109).

Resequencing of Recombinant Viral Stocks

For all bulk (quasispecies-containing) recombinant viruses, HIV-1 RNA was extracted from viral culture supernatant (QIAamp viral RNA kit; Qiagen), amplified and sequenced as described in[4] and compared to the original plasma HIV-1 RNA sequences (Fig. 1). All viruses were confirmed as subtype B using RIP (http://www.hiv.lanl.gov). Nucleotide alignments were performed using GeneCutter and maximum-likelihood phylogenetic trees were generated using PHYml[31] (both available at http://www.hiv.lanl.gov). Trees were visualized using Figtree v.1.2.2 (http://tree.bio.ed.ac.uk/software/figtree/). Resistance mutations were identified using the Stanford HIV Drug Resistance Database (http://hivdb.stanford.edu/). Most controller-derived RT–Integrase sequences were previously deposited in Genbank.[4] Accession numbers for the remaining sequences from controllers and progressors are GQ284657-GQ284730.

Statistical Analysis

Student *T* test was used to compare differences in RC between groups (eg, controllers/progressors; presence/absence of HLA alleles, etc). Spearman and Pearson correlation was used to investigate the relationship between clinical parameters (CD4/pVL) and the presence of HLA-associated escape mutations, respectively, and viral RC. In an exploratory analysis, the Mann-Whitney *U* Test was used to identify specific amino acids in RT–integrase associated with RC; here, *Q* values were used to address multiple tests.[32]

RESULTS

Generation of Recombinant Viruses Expressing RT–Integrase Sequences From Controllers and Progressors

Recombinant viruses were generated using bulk patient plasma-derived PCR amplicons containing RT and integrase sequences and stocks harvested during the early phase of exponential viral spread as described in Methods. For elite controllers (n = 58), the median time to harvest was 25 days

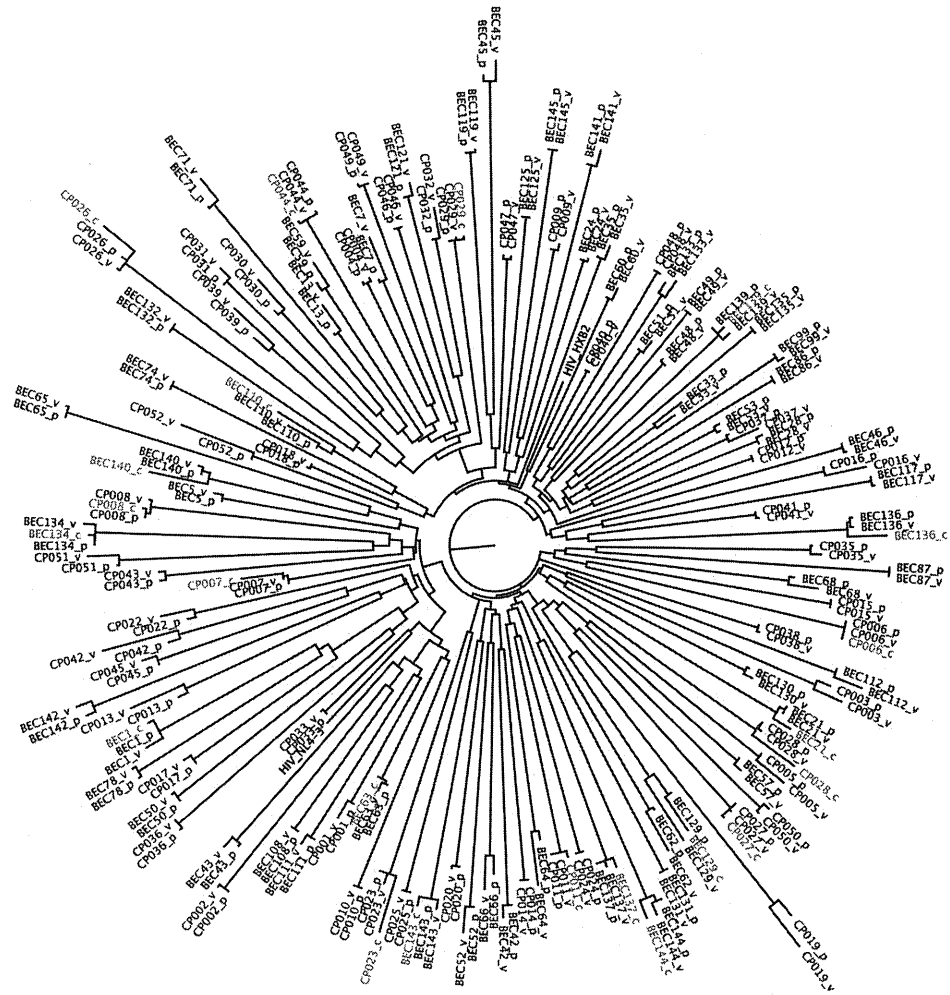

FIGURE 1. Phylogenetic tree illustrating the relationship between HIV-1 RT-Integrase sequences from plasma and recombinant viruses from study subjects. Prefixes "BEC" and "CP" discriminate sequences from controllers and progressors, respectively. Red (suffix "p"), blue (suffix "v"), and green (suffix "c") sequences indicate bulk plasma, bulk recombinant, and clonal recombinant virus sequences, respectively. The sequences of HIV-1 subtype B reference strains HXB2 and NL43 are included for comparison.